

Finding Cliques in Geometric Intersection Graphs with Grounded or Stabbed Constraints

J. Mark Keil and Debajyoti Mondal

Department of Computer Science, University of Saskatchewan, Saskatoon, Canada

Abstract

A geometric intersection graph is constructed over a set of geometric objects, where each vertex represents a distinct object and an edge connects two vertices if and only if the corresponding objects intersect. We examine the problem of finding a maximum clique in the intersection graphs of segments and disks under grounded and stabbed constraints. In the grounded setting, all objects lie above a common horizontal line and touch that line. In the stabbed setting, all objects can be stabbed with a common line.

- We prove that finding a maximum clique is NP-hard for the intersection graphs of upward rays. This strengthens the previously known NP-hardness for ray graphs and settles the open question for the grounded segment graphs. The hardness result holds in the stabbed setting.
- We show that the problem is polynomial-time solvable for intersection graphs of grounded unit-length segments, but NP-hard for stabbed unit-length segments.
- We give a polynomial-time algorithm for the case of grounded disks. If the grounded constraint is relaxed, then we give an $O(n^3 f(n))$ -time $3/2$ -approximation for disk intersection graphs with radii in the interval $[1, 3]$, where n is the number of disks and $f(n)$ is the time to compute a maximum clique in an n -vertex cobipartite graph. This is faster than previously known randomized EPTAS, QPTAS, or 2 -approximation algorithms for arbitrary disks. We obtain our result by proving that pairwise intersecting disks with radii in $[1, 3]$ are 3 -pierceable, which extends the 3 -pierceable property from the long known unit disk case to a broader class.

1 Introduction

Let \mathcal{S} be a set of geometric objects. A *geometric intersection graph* $G(\mathcal{S})$ is a graph where each vertex represents a distinct object in \mathcal{S} and an edge connects two vertices if and only if the corresponding objects intersect. In this paper we consider the problem of finding a maximum *clique* in $G(\mathcal{S})$, i.e., a largest set of pairwise intersecting objects from \mathcal{S} . A rich body of research has examined the maximum clique problem for intersection graphs of various types of geometric objects [8, 15, 26, 29, 33]. In this paper we consider geometric objects in \mathbb{R}^2 and primarily focus on segments and disks.

Intersection Graphs of Segments. The maximum clique problem on the segment intersection graph was first posed as an open problem by Kratochvíl and Nešetřil [35] and remained unresolved

This work was supported by Natural Sciences and Engineering Research Council of Canada (NSERC) through a Discovery grant and an Alliance grant.

for two decades. It was widely regarded as a challenging open problem [5] and finally in ESA 2012, Cabello, Cardinal, and Langerman [14] settled the problem by proving the NP-hardness for computing a maximum clique in ray intersection graphs. A rich body of research examines generalizations of segment graphs, e.g., *string graphs*, which are intersection graphs of curves in the plane. In SODA 2011, Fox and Pach [28] gave a subexponential time algorithm for computing a maximum clique in k -intersecting string graphs. Here a string graph is called *k -intersecting* if every pair of strings have at most k common points. Therefore, the result applies to segment intersection graphs. They also gave a polynomial-time algorithm to approximate the size of a maximum clique in a k -intersecting string graph within a factor of $n^{1-\epsilon_k}$, where $\epsilon_k > 0$ is a parameter that depends on k . They did not provide any detailed derivation for ϵ_k , which relies on the property of specific separators in k -intersecting graphs. To the best of our knowledge, this is still the best known approximation for maximum clique in segment intersection graphs.

Disk Intersection Graphs. In 1990, Clark, Colbourn and Johnson [21] showed that the maximum clique problem is polynomial-time solvable in the case of unit disk graphs. Subsequent research attempted to accelerate the algorithm [11, 23, 25]; however, extending this result to disk graphs with even two distinct radii types remained open for a decade [12, 13]. In SoCG 2025, Keil and Mondal [33] settled this open problem showing that a maximum clique can be computed in polynomial time for disk intersection graphs with a fixed number of radii types. However, the time-complexity question remains open for general disk graphs [27, 3], even when the disk radii are restricted to lie within the interval $[1, 1 + \epsilon]$ for some $\epsilon > 0$ [9]. The maximum clique problem is NP-hard for the intersection graph of ellipses [3], where the ratio of the larger over the smaller radius is some prescribed number larger than 1. However, this hardness result applies neither to the segments nor to the disks.

Grounded and Stabbed Settings. In this paper we consider the maximum clique problem for segment and disk intersection graphs under grounded and stabbed settings. In the grounded setting, all objects lie above a common horizontal line ℓ and touch ℓ . In the stabbed setting, all objects can be stabbed with a common line. Such restrictions have been widely studied in the literature across various problems with the goals of understanding the structure of specific subclasses [16, 31, 19, 17], designing efficient approximation algorithms for the general case [20, 1], and understanding the gap between polynomial-time solvable and NP-hard variants [10, 4, 32, 37].

A pioneering result on the maximum clique problem in intersection graphs of grounded segments was established by Middendorf and Pfeiffer [39]. They showed that the problem is polynomial-time solvable for grounded segments if the *free endpoints*, which are not on the ground line, lie on a fixed number of horizontal lines. They also showed that the problem is NP-hard for intersection graphs of one-bend polylines. Later, Keil, Mondal and Moradi [34] established NP-hardness for grounded one-bend polylines, even when their free endpoints and bends are restricted to lie on two horizontal lines. They posed the open question of whether the case of grounded segments is polynomial-time solvable, which was later asked even under the stricter condition where the grounded segments are of unit length [2]. The NP-hardness result for grounded one-bend polylines naturally applies to the stabbed setting. Similarly, the NP-hardness for ray intersection graphs [14] can be seen as the case where all segments are grounded on a circle or stabbed by a circle.

To the best of our knowledge, the intersection graphs of grounded disks have remained unexplored, but several studies have considered various forms of stabbing. For example, Breu [11] studied unit disk graphs with the restriction when all disks lie within a strip of width $\sqrt{3}/2$, and here the disks can be stabbed by the bisector line of the strip. Another widely studied setting is point stabbing or piercing. Every set of mutually intersecting disks can be pierced by four points [18, 22, 41], and three points suffice for unit disks [6, 30]. This idea is useful for designing a 2-approximation in

$O(n^4 \cdot f(n))$ time [3] for n disks as follows. First, compute the arrangement \mathcal{A} of the disks, and then compute for each pair of cells $c, c' \in \mathcal{A}$, a maximum clique in the intersection graph $G(c, c')$ of the disks hit by c, c' . Here $f(n)$ is a polynomial in n , which represents the time to compute a maximum clique in the cobipartite graph $G(c, c')$. A subexponential-time QPTAS and a randomized EPTAS were developed in FOCS 2018 [8], but both are slower than the straightforward 2-approximation.

Contributions. In this paper we show that finding a maximum clique is NP-hard in the intersection graphs of upward rays. This implies NP-hardness both for grounded segments and for unit-length segments that are stabbed by a line, which settles the time-complexity question posed in [34]. The NP-hardness reduction is achieved by showing that every planar graph G has an even subdivision whose complement can be represented as an upward ray graph, whereas the previous NP-hardness result for ray graphs [15] used both upward and downward rays to find a geometric representation for G . The construction of rays in [15] relies on a symmetric ray arrangement around a circle, making it unclear how to adapt the method to enforce upwardness of the rays. Instead, we give an incremental construction in which each newly inserted ray is carefully rotated so that all rays remain upward.

In contrast, we give polynomial-time algorithms for two restricted cases. One is for grounded unit-length segments, which settles the time-complexity question posed in [2]. Here we reduce the problem to computing a maximum clique in a cocomparability graph, which is known to have a polynomial-time solution [29]. The other is for grounded segments with the free endpoints lying on $O(1)$ lines, which strengthens the result of [39] that assumes free endpoints to be on horizontal lines. Since we allow lines that are not necessarily horizontal, the dynamic programming approach of [39], which relies on subproblem decomposition using the heights of the horizontal lines, no longer applies. Our algorithm also employs a dynamic program, but to handle lines of arbitrary slopes, we prove that only a few segments per line need to be tracked when performing the subproblem decomposition. For intersection graphs of arbitrary grounded segments, we give an $O(n^{3/4})$ -approximation for the size of a maximum clique in polynomial time using a simpler approach than that of [28].

For grounded disks, we give a polynomial-time solution to compute a maximum clique. If the grounded constraint is relaxed, then we compute a $3/2$ -approximation for $[1, 3]$ -disks in $O(n^3 \cdot f(n))$ -time. Here $f(n)$ is the time to find a maximum clique in an n -vertex cobipartite graph. Although we impose restriction on radii, the running time is faster than the previously known 2-approximation algorithm [3], QPTAS, and randomized EPTAS [7] that work for arbitrary disks. However, the central contribution here is our underlying proof that every set of pairwise intersecting $[1, 3]$ -disks can be pierced by 3 points. This extends the 3-pierceable property, which was long known for unit disks [6, 30], to the broader class of $[1, 3]$ -disks.

The following table gives a summary of the contribution.

Objects → Setting ↓	Upward Rays/ Segments	Unit- Length Segments	Segments with Endpoints on $O(1)$ lines	Disks
Grounded	NP-hard – Th. 2.2 $O(n^{3/4})$ -approx. Th. 3.8	Poly-time Th. 3.7	Poly-time Th. 3.4	Poly-time – Th. 4.1
Stabbed by Line	NP-hard Th. 2.2	NP-hard Th. 2.2	Open	$3/2$ -approx. for $[1, 3]$ -disks in $O(n^3 f(n))$ -time – Th. 4.9

2 NP-Hardness for Intersection Graphs of Upward Rays, Grounded Segments, and Stabbed Unit-Length Segments

In this section we show that the maximum clique problem is NP-hard for intersection graphs of upward rays. Every graph admitting an upward ray representation also has a grounded segment or stabbed unit-length segment representation, as follows. Given an upward ray representation, consider a horizontal line L with sufficiently high y -coordinate such that all intersection points of the rays are below L , remove the parts of the rays that are above L , flip the representation vertically, and treat L as the ground line. To obtain a unit-length segment representation, we extend the segments below L so that all segments obtain the same length. Since all intersection points of the rays were on the other side of L , the extended parts do not create any new intersection point. Consequently, our NP-hardness result implies NP-hardness for intersection graphs of grounded segments and stabbed unit-length segments.

The proof idea is to show that every planar graph has an even subdivision whose complement has an intersection representation with upward rays. Since finding an independent set in an even subdivision of a planar graph is NP-hard [15], we obtain the NP-hardness for the maximum clique problem on upward ray graphs. We first briefly describe the required subdivisions of planar graphs (used in [15]), and then prove that they are intersection graphs of upward rays. When constructing the upward ray representation, we do not enforce polynomially bounded coordinates. Therefore, our NP-hardness result holds under the assumption that the input is given as a combinatorial representation of upward ray graphs, rather than a geometric representation.

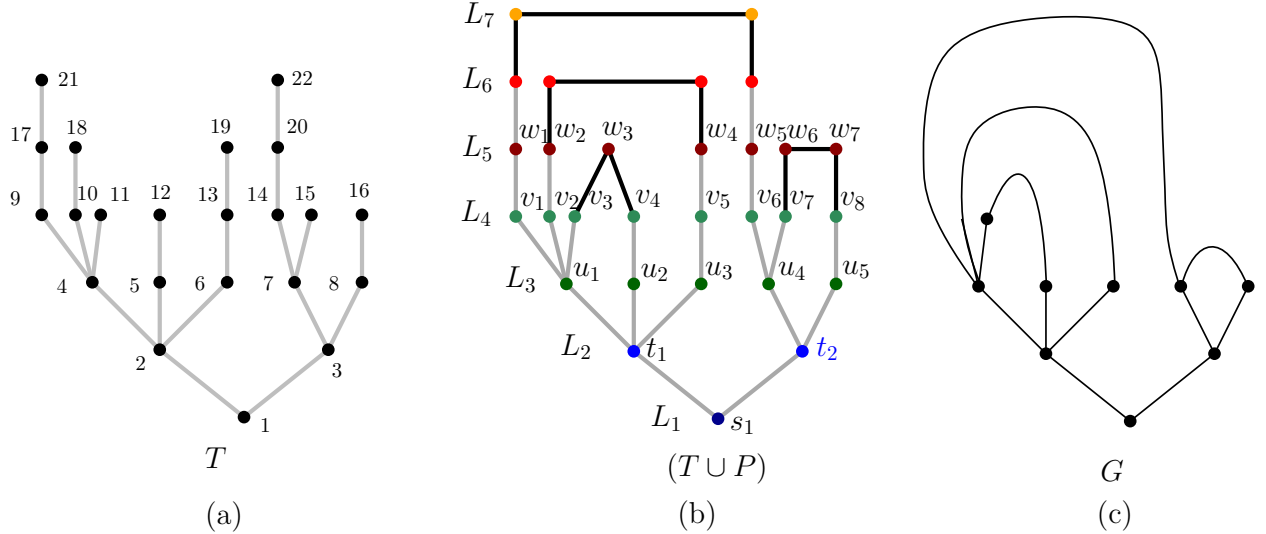


Figure 1: (a) An embedded tree. (b) An even subdivision of $(T \cup P)$, where T and P are shown in gray and black, respectively. (c) The planar graph underlying $(T \cup P)$.

2.1 Even Subdivisions of Planar Graphs

Let T be an embedded tree and let σ be the order of its nodes in breadth-first traversal that starts at the root and visits its children in clockwise order, and then at each internal node, considers its children in clockwise order starting from its parent. Figure 1(a) illustrates an embedded tree where nodes are ordered using such a breadth-first traversal. By *the i th level* of T , where $i \geq 1$, we denote

the ordered subset of nodes from σ that are at distance $(i - 1)$ from the root of T . By σ_i we denote the ordered sequence of vertices at the i th level.

An *admissible extension* of T is a set P of vertex-disjoint paths with the following properties: (a) Each maximal path in P has 3 or 4 vertices. (b) The endpoints of each maximal path in P are leaves of T that are consecutive and at the same level. (c) The internal vertices of any path in P are not vertices of T .

Figure 1(b) shows an admissible extension of a tree T , where the edges of T are shown in gray and the edges of P are shown in black, respectively. By $\overline{(T \cup P)}$ we denote the complement of the graph $(T \cup P)$. An *even subdivision* of a graph G is a graph G' that for each edge (u, v) of G , either retains the edge or replaces it with a path of even number of division vertices. We will use the following lemma.

Lemma 2.1 (Cabello, Cardinal, and Langerman [15]) *Any embedded planar graph G has an even subdivision $(T \cup P)$, where T is an embedded tree and P is an admissible extension of T . Furthermore, such T and P can be computed in polynomial time.*

2.2 Computing an Upward Ray Representation of $\overline{(T \cup P)}$

We now show that $\overline{(T \cup P)}$ (obtained by taking the complement of $(T \cup P)$) admits an intersection representation with upward rays. We begin by introducing some notation that will be used throughout the construction. Let r be a ray with origin q . Let h_q be a horizontal line through q . We say r is *upward* if it has a non-zero slope and lies above h_q . Let A be an arrangement of a set of rays (Figure 2(a)). By a *face* or a *cell* of A we denote a connected region of the plane delimited by the rays of A . By a *path* of A we denote a simple polygonal chain in A . A path is called an *outerpath* if all its segments lie on the unbounded face of A . A *sail configuration* \mathcal{S} of size k is an arrangement of k mutually intersecting rays r_1, \dots, r_k that contains an outerpath e_1, \dots, e_k , where for each i from 1 to k , e_i is a part of r_i (Figure 2(b)). We refer to e_1, \dots, e_k as the *extremal path* of \mathcal{S} . A sail is called *upward* if it consists only of upward rays. We will often add a sail \mathcal{S}' on top of another sail \mathcal{S} such that each ray r'_i of \mathcal{S}' originates at the cell immediately above the edge e_i on the extremal path of \mathcal{S} (Figure 2(c)). Since r'_i intersects all the other rays except for r_i , this realizes the complement of a matching.

We are now ready to describe the details. We first refer the reader to Figure 1(b) which illustrates an even subdivision $(T \cup P)$ of a planar graph, and Figure 2(d) that shows a high-level sketch for the construction. We start with two upward sail configurations \mathcal{S}_ℓ and \mathcal{S}_r of $\lceil k/2 \rceil + 1$ rays, where k is the number of levels of T . We label the rays of $\mathcal{S}_\ell = (L_1, L_3, \dots)$ and $\mathcal{S}_r = (L_2, L_4, \dots)$ with odd and even indices, respectively. Figure 1(d) shows the first three rays of \mathcal{S}_ℓ and \mathcal{S}_r in thick and thin rays, respectively. We refer to these two sails as the *sail skeleton*, and their rays as *skeleton rays*, which will guide the construction of the rays corresponding to $(T \cup P)$. For simplicity of presentation, we define more skeleton rays than the number of levels in T . Consequently, some of the high-index skeleton rays may remain unused and can be removed after the complete construction. Assume that $k' = \lceil k/2 \rceil + 1$. We define L_1 to be an upward ray starting at origin with $(90^\circ + \alpha)$ angle of inclination, where $\alpha = 90^\circ/2k'$. For each i from 2 to $2k'$, the origin of L_i lies on L_{i-1} , and L_i intersects all other skeleton rays. We include the detailed construction of a sail skeleton in Appendix A.

2.2.1 Construction of the Rays Corresponding to the Nodes of T

The skeleton ray L_1 represents the root of T . Let γ be the smallest distance over all pairs of distinct intersection points in the sail skeleton. For each skeleton ray L_i , where $1 \leq i \leq 2k'$, we

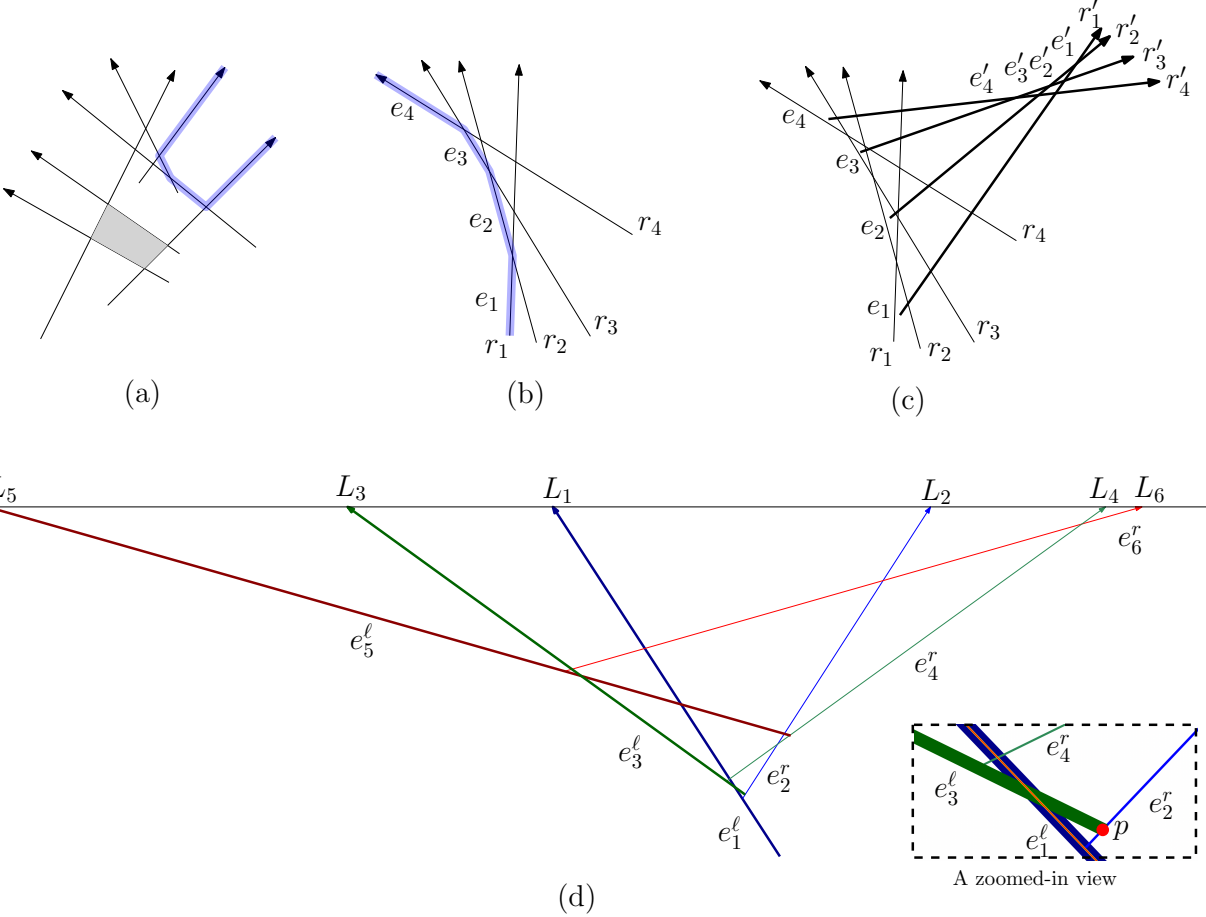


Figure 2: (a) Illustration for a face of A in gray and an outerpath in blue shade. (b) An upward sail S , where the extremal path is in blue. (c) An upward ray representation of a complement of a matching using two sails. (d) An illustration for the sail skeleton.

now consider a strip L_i^s of width ϵ , chosen sufficiently small relative to γ , so that the thickened rays do not completely cover any face of the sail skeleton.

By $\xi(j)$, where $j \geq 2$, we denote the parallelogram determined by L_{j-1}^s and L_j^s (Figure 3). For each j th level of T , where $j \geq 2$, we now construct a sail configuration R_j with $|\sigma_j|$ upward rays such that the origins of these rays remain bounded within $\xi(j)$ and all intersection points of the sail remain within $\xi(j+1)$. We will initially make all rays of R_j to pass through a common point, and then move the rays to ensure a non-degenerate extremal path.

Let u_1, \dots, u_r be the vertices in σ_{j-1} and let e_1, \dots, e_r be the extremal path of sail R_{j-1} (Figure 3). For each t from 1 to r , we construct $c(u_t)$ upward rays, where $c(u_t)$ is the number of children of u_t . The origin of these rays lie inside the cell immediately above e_t and the rays pass through the centroid of $\xi(j+1)$. For example, the vertex u_4 in Figure 3 has two children v_6, v_7 , and thus the origins of their rays lie in the cell immediately above e_4 .

We now consider a vertex v in σ_j and verify its adjacencies. Since we are realizing $\overline{(T \cup P)}$, the ray for v must intersect all rays corresponding to $\sigma_1, \dots, \sigma_j$ except for the ray representing its parent u_t in T . By the construction of the initial sail skeleton, the ray of u_t intersects all rays corresponding to the vertices in $\sigma_1, \dots, \sigma_{j-2}$. Since the ray corresponding to v starts at the cell immediately above e_t , it intersects all the rays corresponding to $\sigma_{j-1} \setminus u_t$. Finally, since the rays of

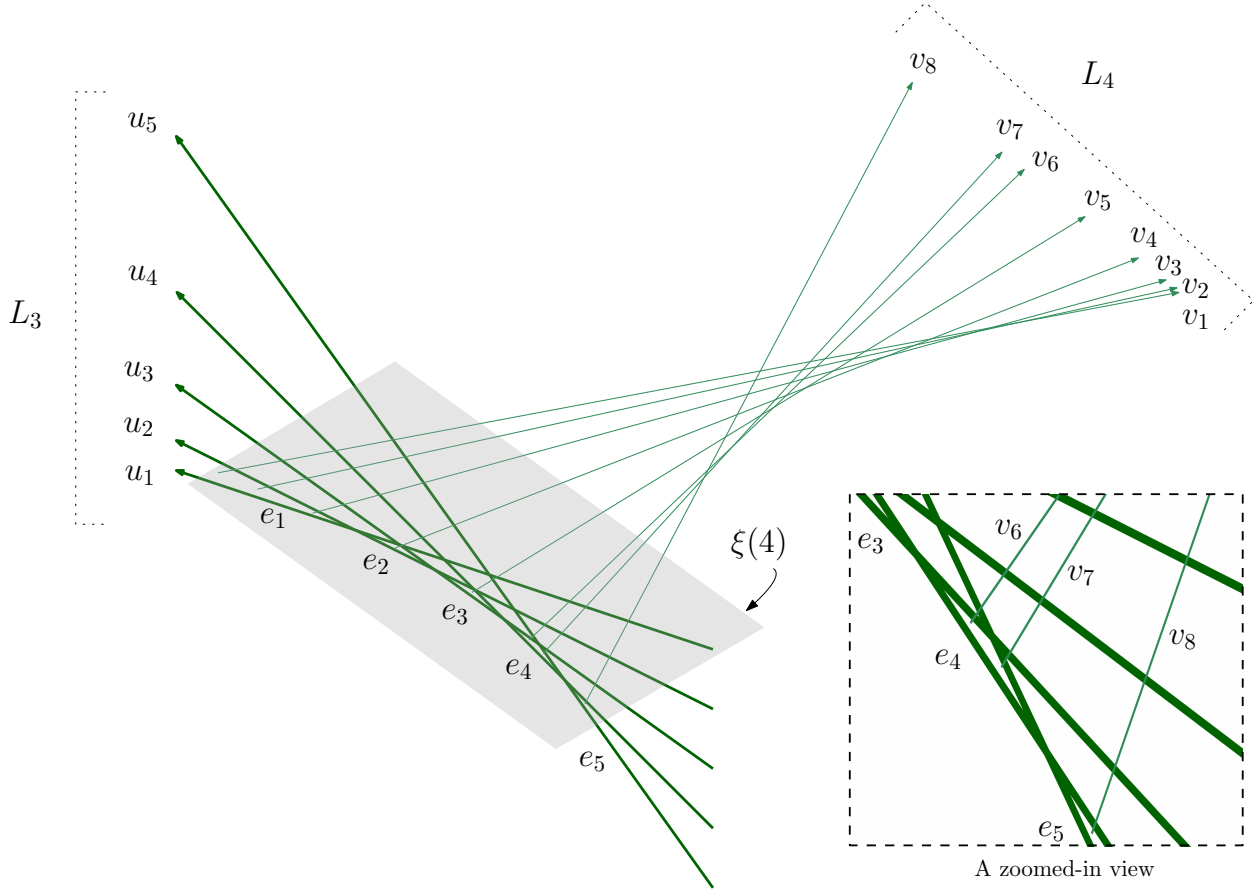


Figure 3: Construction of the vertices of two consecutive levels.

R_j pass through a common point of $\xi(j+1)$, the adjacencies for v have been correctly realized. We now move the rays of R_j (without changing origins) to obtain a non-degenerate sail configuration R_j whose intersection points all lie within $\xi(j+1)$. Since we do not require polynomially bounded coordinates, it is straightforward to move the rays one at a time in the same order as in σ_j to obtain such a representation (Appendix B).

2.2.2 Construction of the Rays for the Internal Nodes of P

The rays for the internal nodes of $P = (a, b, c, d)$ can be inserted in almost the same way as in the previous section. By definition of an admissible extension, the rays of a, d appear consecutively on an extremal path, and hence the rays for b, c can be constructed in the cell immediately above the edges e_a and e_d corresponding to a, d . Figure 4 illustrates an example where $P = (v_7, w_6, w_7, v_8)$. The details are included in Appendix C.

The following theorem summarizes the result of this section.

Theorem 2.2 *Finding a maximum clique is NP-hard for the intersection graphs of upward rays, grounded segments, and stabbed unit-length segments.*

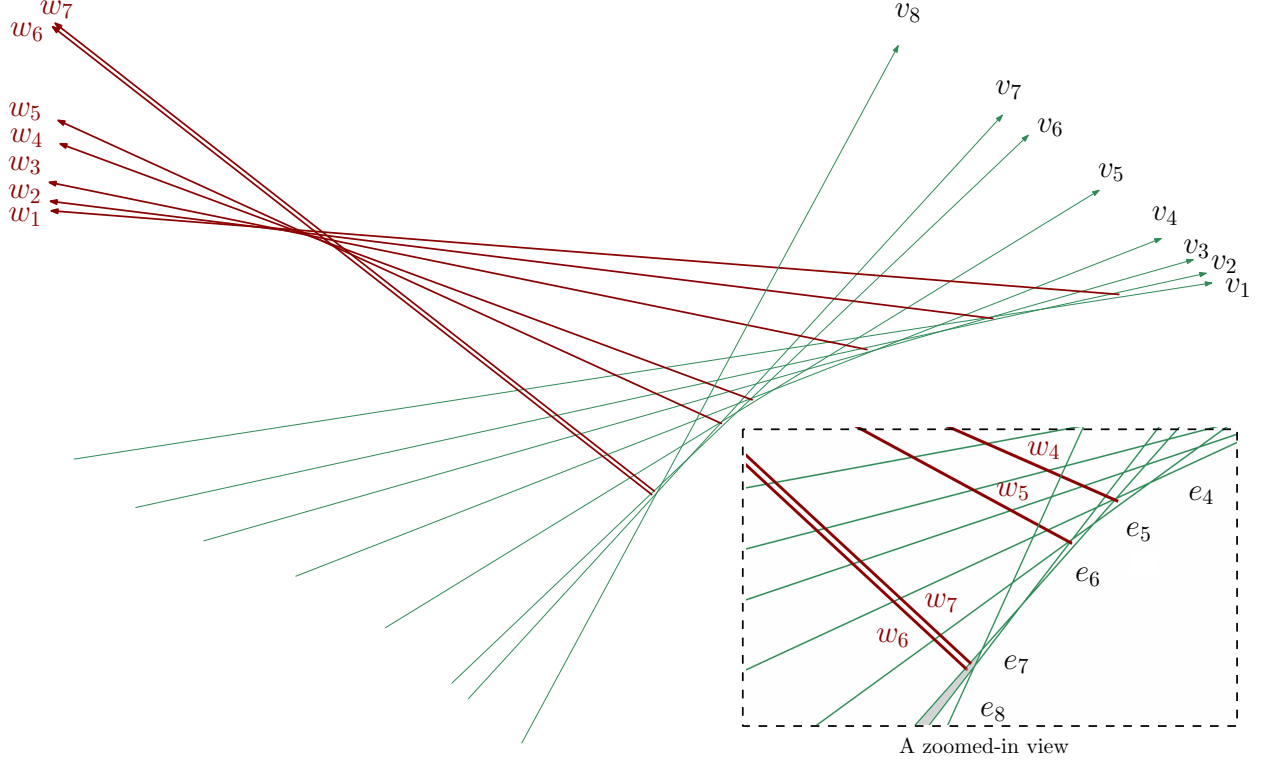


Figure 4: Illustration for the representation of some paths in P .

3 Approximation Results and Exact Computation

In this section we give polynomial-time algorithms to compute a maximum clique in an intersection graph of grounded segments in two restricted cases. We then give a polynomial-time algorithm that achieves an $O(n^{3/4})$ -approximation.

3.1 Segments with Endpoints on Fixed Line Set

The origin of the rays that we used to show NP-hardness for segment graphs cannot be covered with $O(1)$ lines. Therefore, our hardness result does not hold if we restrict the endpoints of the segments to lie on a fixed number of lines. We now show that such restrictions allow us to design a polynomial-time algorithm to find a maximum clique in an intersection graph of grounded segments. However, the time-complexity for the stabbed setting under this restriction remains open. For simplicity of presentation, we assume that the endpoints of the segments are distinct.

The idea is to design a dynamic programming algorithm by introducing a concept of strict independent set. We define a pair of grounded segments to be *strictly independent* if they satisfy the following conditions: (C_1) The segments do not intersect. (C_2) Extending either of the segments beyond the free endpoint (above the ground line) does not create an intersection with the other. However, if both segments are extended beyond their free endpoints, the extended parts intersect each other.

The pairs of segments in Figures 5(a)–(c) are not strictly independent, whereas Figure 5(d) illustrates a strictly independent pair. A *strict independent set* is a collection of grounded segments where every pair is strictly independent. We first transform the input grounded segments S into another set of grounded segments S' such that a strict independent set in $G(S')$ corresponds to a

maximum clique in $G(S)$.

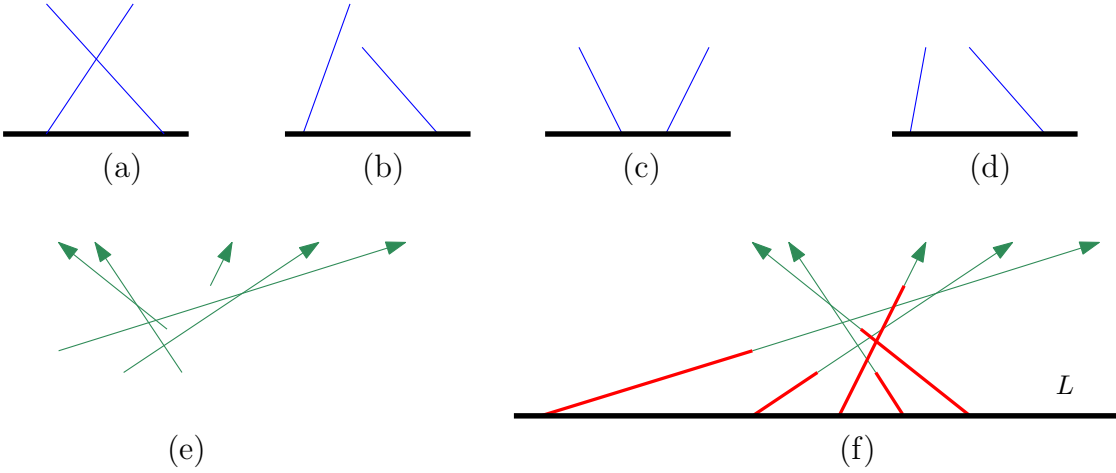


Figure 5: (a)–(c) Pairs that are not strictly independent. (d) A strictly independent pair. (e) An upward ray representation. (f) A corresponding grounded segment representation in red.

3.1.1 Transforming S into S'

We use the result of [17] to transform the segments of S into a set of upward rays $U(S)$ such that two segments of S intersect if and only if the corresponding rays of $U(S)$ intersect. Figure 5(e) gives an example for $U(S)$. Such a transformation can be done in linear time.

We now consider the arrangement \mathcal{A} of lines determined by the rays in $U(S)$ and define a ground line L such that all the intersection points of the arrangement lie above L . We now create the set S' by considering the parts of the lines that are between the ground line L and the rays in $U(S)$. Figure 5(f) illustrates S' in red. We now have the following lemma with the proof in Appendix D.

Lemma 3.1 *A pair of segments in S intersect if and only if the corresponding segments in S' are strictly independent.*

3.1.2 Dynamic Program to Compute a Strict Independent Set of S'

Assume that the lines ℓ_1, \dots, ℓ_k cover all the free endpoints of the segments in S' . We define the *height of a segment* s to be the y -coordinate of its free endpoint and denote the height by $h(s)$. Let $\sigma[1 \dots n]$ be a sequence of segments obtained based on their order on the ground line. We use the terms left and right to describe the relative order of segments in σ . The idea of the algorithm is to order the segments in non-decreasing order of heights. The algorithm will use this order to guess the segments in the optimal solution. Assume that a set I of strictly independent segments has already been selected. To extend this set while maintaining strict independence, the algorithm generates subproblems by guessing the next tallest segment to include and takes the maximum over all such choices. Another key component of the algorithm is a compact problem encoding. Instead of retaining all the segments of I , we will maintain a set of at most $4k$ segments to pass to each subproblem.

We first introduce some notation and preliminary observations. Let s_i, s_j be two segments where s_i is to the left of s_j in σ . Let T be a strict independent set of at most $4k$ segments, where at most $2k$ lie in $\sigma[1 \dots i]$ and at most $2k$ lie in $\sigma[j \dots n]$. By $Q[s_i, s_j, T]$ we denote the maximum

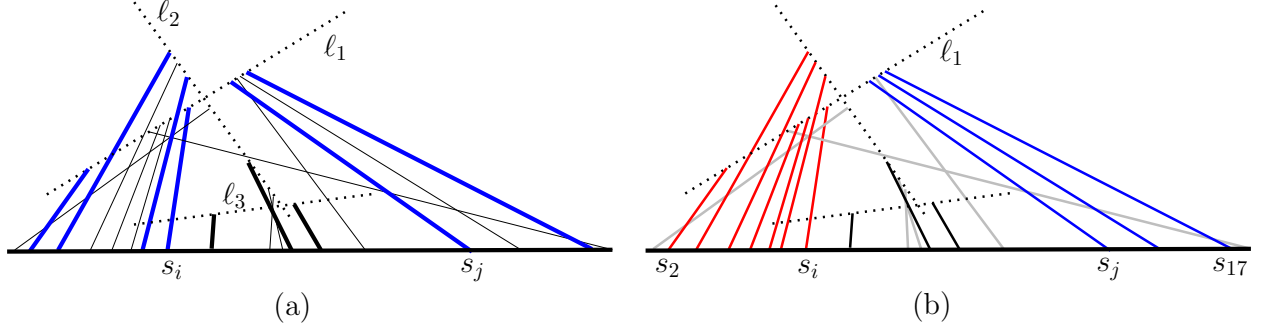


Figure 6: (a) A set of grounded segments with free endpoints covered by 3 lines (shown in dots). A set T is shown in thick blue, and the segments corresponding to $Q[s_i, s_j, T]$ are shown in thick black. (b) Illustration for A'_l , A'_r and A' in red, blue, and black, respectively.

number of segments that can be added from $\sigma[i+1 \dots j-1]$, where no segment is higher than both s_i, s_j , and together they form a strict independent set with T (Figure 6(a)).

Let A be a maximum strict independent set in S' . Let s_i and s_j be two segments in A such that no segment of A between s_i and s_j is higher than both s_i, s_j . Let A' be the set of these segments. Let \overline{A}'_l and \overline{A}'_r be the segments of $(A \setminus A')$ that lie to the left and right of A' , respectively (Figure 6(b)). We now construct a strict independent set T as follows. For each w from 1 to k , we fill the entries $T[4w-3 \dots 4w]$ from segments of $(A \setminus A')$ that have free endpoints on ℓ_w . Specifically, the first two entries $T[4w-3]$ and $T[4w-2]$ are set to the highest and lowest segments of \overline{A}'_l that have free endpoints on ℓ_w . Similarly, $T[4w-1]$ and $T[4w]$ are set to the highest and lowest segments of \overline{A}'_r that have free endpoints on ℓ_w . If we do not find enough segments to assign, then some of these entries remain null. It is straightforward to observe by the construction of T that s_i and s_j belong to T . For example, in Figure 6(b), the entries $T[1, \dots, 4]$ are set to s_i, s_2, s_{17}, s_j , respectively.

The following lemma justifies the problem encoding, whose proof is in Appendix E.

Lemma 3.2 *Let A be a maximum strict independent set in S' , and let s_i and s_j be two segments in A . Let A' be the set of the segments of A that lie between s_i and s_j . Assume that no segment of A' is higher than both s_i, s_j . Let Z be the segments corresponding to $Q[s_i, s_j, T]$. Then $Z \cup (A \setminus A')$ is a maximum strict independent set of S' .*

By Lemma 3.2, instead of tracking the entire set $(A \setminus A')$ that has already been taken in the solution, we can encode the subproblems with respect to a subset T of $(A \setminus A')$, i.e., $Q[s_i, s_j, T]$. We now formulate a recurrence relation for $Q[s_i, s_j, T]$. For convenience of presentation, we insert two dummy segments in S' . One to the left of $\sigma[1]$ and the other to the right of $\sigma[n]$ such that the following conditions hold for the newly added segments. (a) They are strictly independent both among themselves and with each segment in S' . (b) They are higher than the segments of S' . (c) Their free endpoints lie on a horizontal line ℓ_{k+1} which is different than ℓ_1, \dots, ℓ_k .

The dummy segments $\sigma[0]$ and $\sigma[n+1]$ can be constructed by first computing a rectangle $abcd$ that encloses all the segments of S' and intersects the extended parts of all the segments in S' at its top side ab . The segments $\sigma[0]$ (resp., $\sigma[n+1]$) are then constructed with a positive (resp., negative) slope with a (resp., b) as its free endpoint. The size of the maximum strict independent set in S' is now $Q[s_0, s_{n+1}, T]$, where $T = \{s_0, s_{n+1}\}$. For simplicity, we write the elements of T without showing the null entries. The following lemma gives a problem decomposition (Figures 7(b)–(d)) whose proof is in Appendix E.

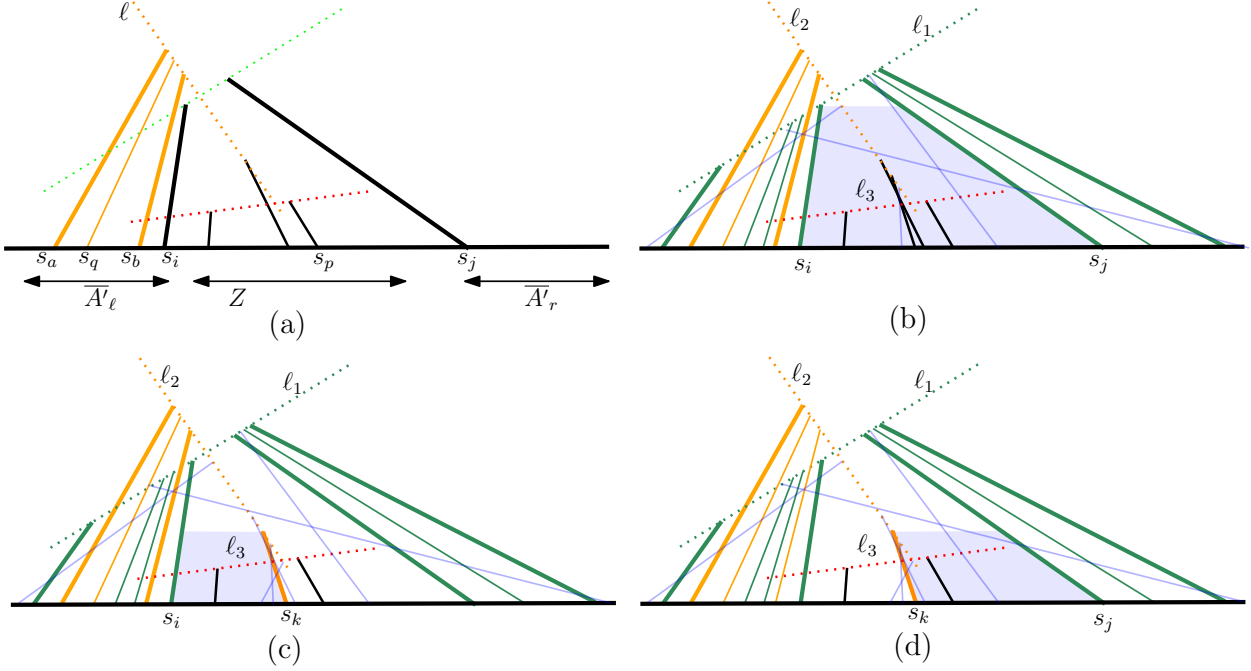


Figure 7: (a) Illustration for Lemma 3.2. (b) A subproblem $Q[s_i, s_j, T]$, where segments that have already been taken in the solution are shown in green or orange depending on whether they are on ℓ_1 or ℓ_2 , respectively. The segments that are not strictly independent with the selected segments are in thin blue. The segments in T are shown in thick orange or green lines. The black segments are candidates for s_k . (c)–(d) A decomposition of $Q[s_i, s_j, T]$ into $Q[s_i, s_k, T_1]$ and $Q[s_k, s_j, T_2]$.

Lemma 3.3

$$Q[s_i, s_j, T] = \begin{cases} 0 & ; \text{if no segment between } s_i, s_j \text{ has} \\ & \text{height at most } \min\{h(s_i), h(s_j)\} \\ & \text{and is strictly independent to } T. \\ \max_{s_k} \{Q[s_i, s_k, T_1] + Q[s_k, s_j, T_2] + 1\} & ; \text{over } s_k \text{ between } s_i, s_j \text{ where} \\ & h(s_k) \leq \min\{h(s_i), h(s_j)\} \text{ and } s_k \\ & \text{is strictly independent with } T. \end{cases}$$

Let ℓ be the line that contains the free endpoint of s_k . Let T^- (T^+) be the entries of T that lie to the left (right) of s_i . If T^- contains two segments s, s' with free endpoints on ℓ , then T_1 is obtained by adding s_k and deleting the segment with median position among s, s', s_k . Otherwise, T_1 is obtained by adding s_k to T . The construction of T_2 is symmetric with respect to T^+ .

Since there are $O(n)$ possibilities for each of s_i and s_j , and $O(n^{4k})$ possibilities for T , the number of subproblems is $O(n^{4k+2})$. By Lemma 3.3, each subproblem can be computed by $O(n)$ table lookup. If $k = O(1)$, the overall running time to compute the solution to all subproblems is $O(n^{O(1)})$. We now use Lemma 3.1 to obtain the following theorem.

Theorem 3.4 *Given a set of n grounded segments whose free endpoints lie on $O(1)$ lines, a maximum clique in the corresponding intersection graph can be computed in $O(n^{O(1)})$ time.*

3.2 Unit-Length Grounded Segments

We now give a polynomial-time algorithm to find a maximum clique in a grounded unit-length segment graph $G(S)$. Let M be a maximum clique of $G(S)$, the idea is to define a set of subgraphs \mathcal{G} of polynomial size such that at least one of them is guaranteed to contain the maximum clique M . The search for M is then confined to these subgraphs. To ensure the feasibility of this approach, we also need to prove that each subgraph has a nice property that allows for finding its maximum clique in polynomial time.

The construction of \mathcal{G} is simple. For a pair s_a, s_b of intersecting grounded segments, let $G(s_a, s_b)$ be the intersection graph determined by all the segments that intersect both s_a and s_b , and lie between s_a and s_b on the ground line. We now define \mathcal{G} to be the set of graphs $\bigcup_{s_a, s_b \in S} G(s_a, s_b)$. Let M be a maximum clique of $G(S)$ and let s_ℓ and s_r be the leftmost and rightmost segments of M , then the clique must exist in the graph $G(s_\ell, s_r)$. We will show that $G(s_\ell, s_r)$ is a cocomparability graph, and hence a maximum clique can be computed in polynomial time [29].

A linear ordering $v_1 \dots, v_n$ of the vertices of a graph is called an *umbrella-free ordering* if for every i, j, k with $1 \leq i < j < k \leq n$, the existence of the edge (v_i, v_k) implies that v_j is adjacent to at least one of v_i or v_k . We will use the following characterization of cocomparability graph.

Lemma 3.5 (Kratsch and Stewart [36]) *A graph is a cocomparability graph if and only if it has an umbrella-free ordering.*

Lemma 3.6 *The graph $G(s_\ell, s_r)$ is a cocomparability graph.*

Proof: [Proof Sketch] Let $\sigma = (s_\ell, \dots, s_r)$ be the order of the segments of $G(s_\ell, s_r)$ on the ground line. We show that σ is an umbrella-free ordering, and thus $G(s_\ell, s_r)$ is a cocomparability graph by Lemma 3.5. Specifically, for every subsequence s_a, s_c, s_b in σ , we show that if s_a and s_b intersect, then at least one of them intersects s_c . We consider two cases based on the location of the intersection point $i(s_a, s_b)$ of s_a and s_b . If $i(s_a, s_b)$ is above both the lines determined by s_ℓ and s_r (Figures 8(a)–(b)), then to avoid s_a, s_b , the length of s_c must be less than one unit. If $i(s_a, s_b)$ is not above both lines (Figures 8(c)–(d)), then to avoid s_a, s_b , the segment s_c must avoid at least one of s_ℓ and s_r . The details are in Appendix G. \square

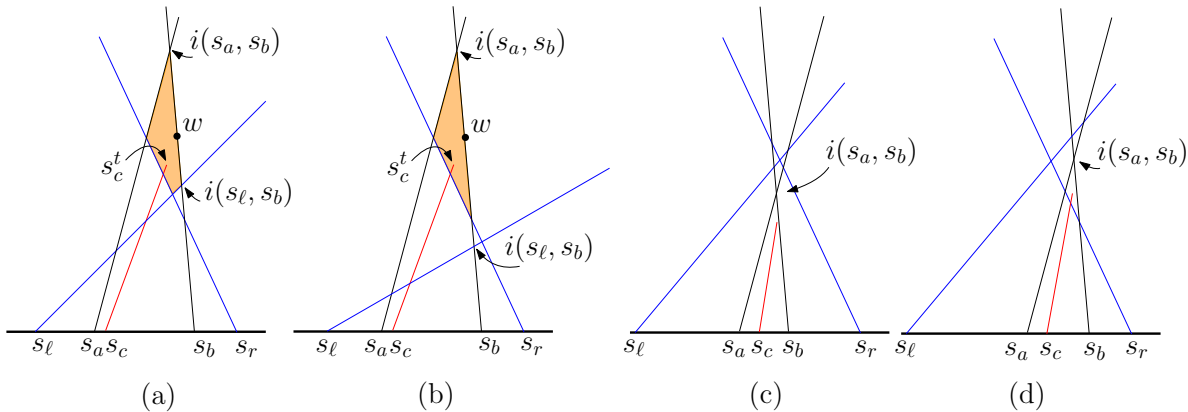


Figure 8: Illustration for the proof of Lemma 3.6. The free endpoint s_c^t of s_c lies in orange region.

Since a maximum clique in an n -vertex cocomparability graph can be computed in polynomial time [29], we can use Lemma 3.6 to obtain the following theorem.

Theorem 3.7 *Given a set of grounded unit-length segments, one can compute a maximum clique in the corresponding intersection graph in polynomial time.*

3.3 Approximation for Grounded Segment Graphs

We now give a polynomial-time $O(n^{3/4})$ -approximation algorithm to compute a maximum clique in an arbitrary grounded segment graph.

Theorem 3.8 *Given n grounded segments, one can compute a clique C in their intersection graph in polynomial time such that $|C|$ is $\Omega(n^{-3/4}|M|)$, where M is a maximum clique.*

Proof: [Proof Sketch] We partition the segments into $O(n^{3/4})$ subsets with specific property. Let S be such a subset and let σ denote an order of its segments in increasing x -coordinates of the free endpoints. We design S such that the corresponding sequence of free (resp., grounded) endpoints is monotonically increasing or decreasing in y -coordinates (resp., x -coordinates). We show that S is a cocomparability graph, which implies that a clique of size $\Omega(n^{-3/4}|M|)$ can be found by examining all subsets. The details are in Appendix F. \square

4 Disk Intersection Graphs

In this section we present the results on disk intersection graphs.

4.1 A Polynomial-Time Algorithm in Grounded Setting

Theorem 4.1 *Given a set of grounded disks \mathcal{D} , a maximum clique in the corresponding disk intersection graph $G(\mathcal{D})$ can be computed in polynomial time.*

Proof: [Proof Sketch] For each disk $D \in \mathcal{D}$, we compute a maximum clique $M(D)$ that contains D as its smallest disk. A maximum clique of $G(\mathcal{D})$ is then obtained by taking the largest among these cliques. To compute $M(D)$, we can only examine the set of disks $S \subseteq \mathcal{D}$ that intersect D . We next show that the intersection graph of S is a cobipartite graph. The details are in Appendix H. \square

4.2 (3/2)-Approximation for [1, 3]-Disk Graphs

In this section we consider $[1, 3]$ -disks, which are disks with radii in the interval $[1, 3]$. Let \mathcal{D} be a set of $[1, 3]$ -disks. We now show how to compute a $3/2$ -approximation in the corresponding disk intersection graph in $O(n^3 f(n))$ time, where $f(n)$ is the time to compute a maximum clique in a n -vertex cobipartite graph. We will use the following observation that given a set of disks pierced by three points, one can compute a $3/2$ -approximation for the maximum clique in $O(f(n))$ time. The idea is to first construct three graphs, each formed by discarding the disks that are uniquely hit one of the three points, and then take the largest clique among the three graphs. To obtain the final approximation algorithm, we will show the search for the maximum clique can be reduced to $O(n^3)$ subsets of mutually intersecting disks.

4.2.1 Piercing Pairwise Intersecting $[1, 3]$ -Disks

Technical Background. We first introduce some notation and preliminary results. We call three pairwise intersecting disks D_1, D_2, D_3 a *Helly triple* if they have a common intersection point. Otherwise, we call them a *non-Helly triple*. The *inscribed circle* of a non-Helly triple is the largest circle that can be contained within the region bounded by the three disks of the triple (Figure 9(a)). Given a line segment ab , we use the notation $L(ab)$ to denote the line determined by ab . For an angle $\angle pqr$, we consider the clockwise angle from qp to qr . By $W(\angle pqr)$, we denote a wedge-shaped

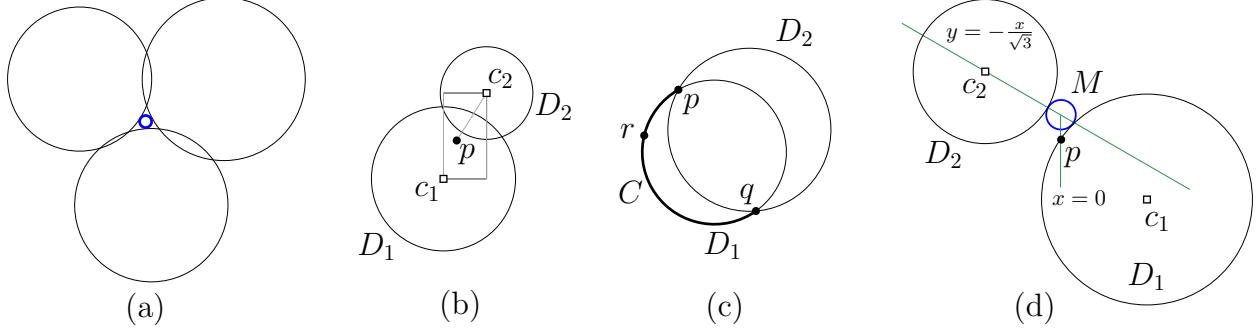


Figure 9: (a) A non-Helly triple and their inscribed circle are shown in black and blue, respectively. Illustration for (b) Lemma 4.3, (c) Lemma 4.4, and (d) Lemma 4.5.

region that is swept by a rotating ray qp clockwise until it aligns with qr . We will use the following four lemmas, where the proof of the last three is included in Appendix I.

Lemma 4.2 (Biniaz, Bose and Wang [6]) *The inscribed circle of a non-Helly triple of three pairwise intersecting disks of radii r has radius at most $r(\frac{2}{\sqrt{3}} - 1)$.*

Lemma 4.3 *Let D_1 and D_2 two intersecting disks with centers c_1 and c_2 , respectively. Let p be a point contained in the axis-aligned rectangle having c_1c_2 as its diagonal (Figure 9(b)). If we move c_2 towards p along $L(pc_2)$, then D_2 maintains the intersection with D_1 .*

Lemma 4.4 *Let D_1 and D_2 be two disks that intersect at two distinct points p and q . Let C be an open circular arc on the boundary of D_1 between p and q , and let r be a point on C (Figure 9(c)). If r lies outside of D_2 , then the entire arc C lies outside of D_2 .*

Lemma 4.5 *Let r be a number in the interval $[1, 3]$. Let M be a circle of radius $r(\frac{2}{\sqrt{3}} - 1)$ with center $o = (0, 0)$ and let p be the point $(0, -\frac{1}{\sqrt{3}})$. Define two disks D_1 and D_2 as follows: D_1 touches p and M with its center lying in the fourth quadrant, and D_2 touches M with its center lying on line $y = -\frac{x}{\sqrt{3}}$ in the second quadrant (Figure 9(d)). If the radii of the disks are at most three, then D_1 cannot intersect D_2 below the line $y = -\frac{x}{\sqrt{3}}$.*

Finding Piercing Points. Let Q be the smallest circle that intersects every disk in \mathcal{D} , which can be computed in linear time [38]. If Q has zero radius, then a single point pierces all disks. Otherwise, Q is an inscribed circle of a non-Helly triple of \mathcal{D} [6]. The following lemma can now be used to find three piercing points A, B, C for the case of unit disks.

Lemma 4.6 (Biniaz, Bose and Wang [6]) *Let S be a set of pairwise intersecting unit disks that contains a non-Helly triple. Assume that the smallest circle that intersects every disk in S is centered at $(0, 0)$. Then the points $A = (0, -\frac{1}{\sqrt{3}})$, $B = (1/2, 1/2\sqrt{3})$ and $C = (-1/2, 1/2\sqrt{3})$ pierce all the disks of S .*

Assume that the smallest circle that intersects all $[1,3]$ -disks of \mathcal{D} is Q , where Q is determined by a non-Helly triple. Let D_b, D_ℓ, D_r be the disks of the non-Helly triple in clockwise order around Q (Figure 10(a)). Let c_b, c_ℓ, c_r, c_q be the centers of D_b, D_ℓ, D_r, Q , respectively. Let o be the origin $(0, 0)$ and assume that $\angle c_\ell o c_r$ is the smallest angle among $\{\angle c_\ell o c_r, \angle c_r o c_b, \angle c_b o c_\ell\}$. We translate \mathcal{D} such that the center of Q coincides with o , and rotate the plane such that c_b lies below o . The following property is known in this setting.

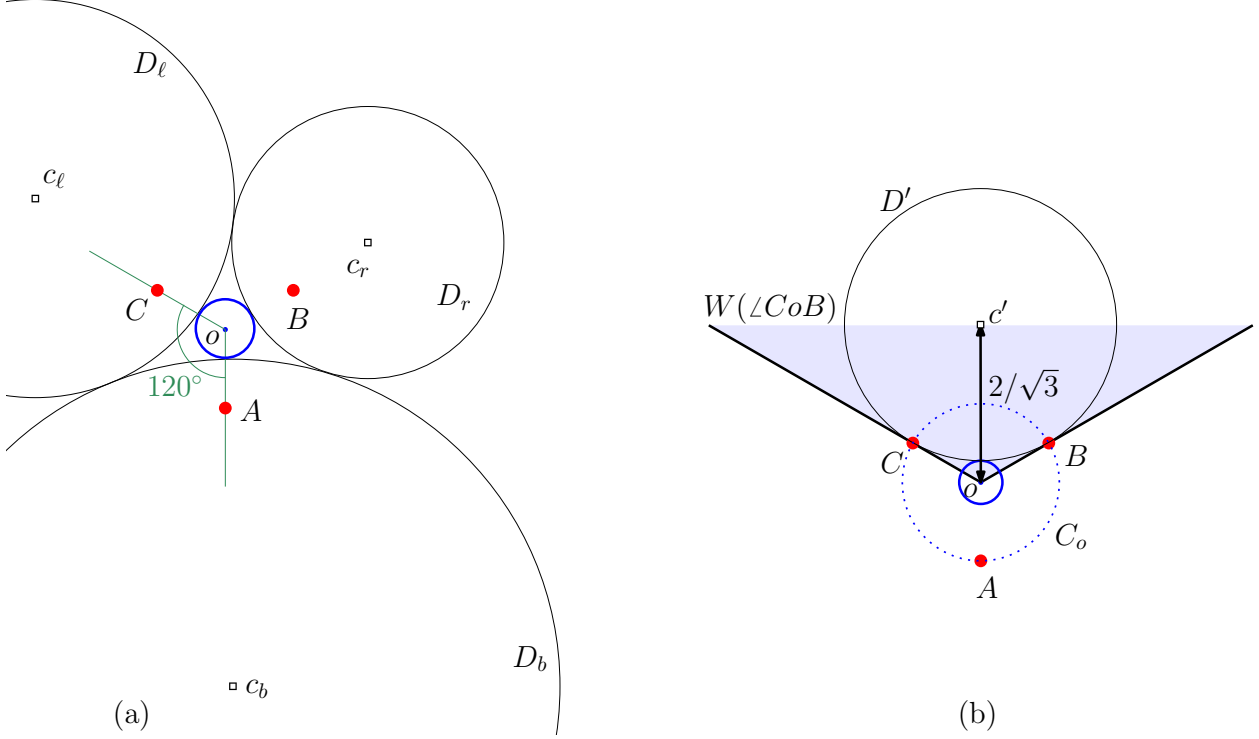


Figure 10: (a) Illustration for $\{D_b, D_\ell, D_r\}$, $\{A, B, C\}$ and Q , where Q is in blue. Some disks are drawn partially for space constraints. (b) A unit disk touching B, C with center in $W(\angle CoB)$.

Lemma 4.7 (Carmi, Katz and Morin [18]) *The tangent at the touching point of D_ℓ and Q has a positive slope and the tangent at the touching point of D_r and Q has a negative slope.*

We now show that the points A, B, C of Lemma 4.6 pierce all disks in \mathcal{D} . Suppose for a contradiction that D' is a disk in \mathcal{D} with center c' and radius r' such that D' is not pierced by any point of $\{A, B, C\}$ but it intersects all three disks D_b, D_ℓ, D_r and Q . Let r_q be the radius of Q . Let C_o be the circle of radius $\frac{1}{\sqrt{3}}$, i.e., a circle that passes through A, B, C .

We first show that r_q must be at least $(\frac{2}{\sqrt{3}} - 1)$ and c' must lie outside of C_o . The three bisectors of pairs of points from $\{A, B, C\}$ meet at o . Therefore, every point inside C_o is within a distance of $\frac{1}{\sqrt{3}}$ from some point of $\{A, B, C\}$. Since D' is not pierced, c' cannot lie in C_o . Assume now that c' lies outside of C_o . Since D' is not pierced, we can move D' such that c' becomes equidistant from two of the points of $\{A, B, C\}$. Without loss of generality assume that c' is equidistant from B and C . If D' is a unit disk, then $|oc'| = \frac{2}{\sqrt{3}}$ (Figure 10(b)). If r_q is smaller than $(\frac{2}{\sqrt{3}} - 1)$, then D' cannot intersect Q . If D' has a larger radius, then it is further away from Q , contradicting that D' intersects Q .

Since the largest radius among the disks of \mathcal{D} is three, the radius of Q is at most $3(\frac{2}{\sqrt{3}} - 1)$ (Lemma 4.2). The remainder of the section assumes that $(\frac{2}{\sqrt{3}} - 1) \leq r_q \leq 3(\frac{2}{\sqrt{3}} - 1)$ and c' is outside of C_o . We now consider two cases based on the location of c' and show that in each case D' is pierced.

Case 1 ($c' \in W(\angle CoB)$). Note that D' cannot contain o . We now assume without loss of generality that D' intersects D_b on the left halfplane of $L(oA)$, and hence below $L(oC)$. We translate D' along the line $L(c'o)$ such that it touches C . Since D' previously intersected D_b and Q , by Lemma 4.3

it continues to intersect D_b and Q during this translation. Since D' intersects D_b and touches C , c' is on the left halfplane of the line $x = C$. We now rotate D' counter-clockwise without changing distance $|c'c|$ such that it touches Q (Figure 11(a)). Let c'_{old} be the position of c' before the rotation. Since c'_{old} is on the left halfplane of the line $x = C$, $\angle c'c'_{old}c_b$ cannot be larger than $\angle c'_{old}c'c_b$. Hence $|c'c_b| \leq |c'_{old}c_b|$, and D' continues to intersect D_b . We now reach a contradiction by Lemma 4.5 considering C, Q, D' and D_b as p, M, D_2 and D_1 , respectively (Figure 11(b)).

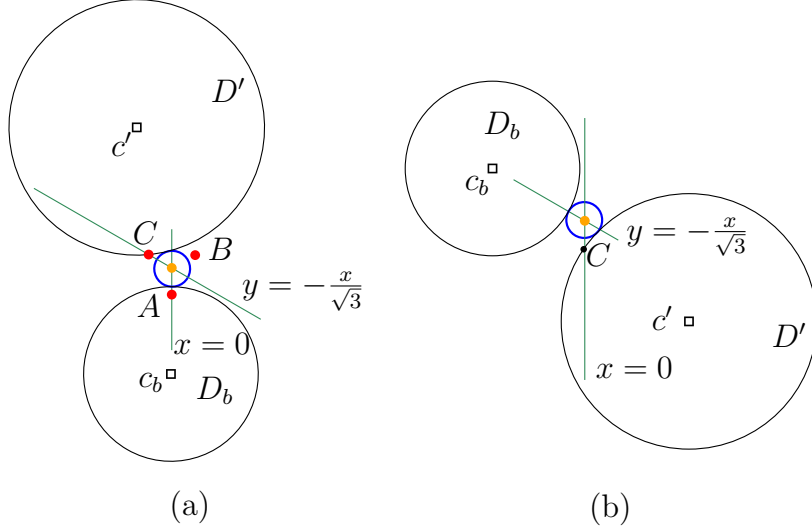


Figure 11: (a) Illustration for Case 1, where Q is shown in blue and o is marked in orange. (b) A transformation of the plane to show the relation to Lemma 4.5.

Case 2 ($c' \in W(\angle AoC)$ or $c' \in W(\angle BoA)$). It suffices to consider the case when $c \in W(\angle BoA)$ because the argument in the other case is symmetric. Since D' cannot contain o , we can consider two subcases depending on whether D' intersects D_ℓ above or below $L(oC)$.

Case 2.1 (D' intersects D_ℓ below $L(oC)$). We handle this case considering the following two scenarios. If c_ℓ lies above $L(oC)$, then we reposition c_ℓ and D' so that c_ℓ lies on $L(oC)$ and D' touches A and Q . We show how to reach a contradiction using Lemma 4.5. If c_ℓ lies below $L(oC)$, then we observe by Lemma 4.7 that D_ℓ touches the upper-left arc of D_b . We then show that D' avoids this arc, and hence avoids D_ℓ . The details are in Appendix I.1.

Case 2.2 (D' intersects D_ℓ above $L(oC)$). The intuition for handling this case is as follows. Since D_ℓ touches D_b , $\angle c_b o c_\ell$ cannot be very large. Furthermore, the constraint that D' must intersect Q and avoid C , pushes D' away from the positive x-axis. We thus reach a contradiction by showing that D' cannot intersect D_ℓ . The details are in Appendix I.1.

The following theorem summarizes the result of this section.

Theorem 4.8 *Let \mathcal{D} be a set of n pairwise intersecting disks with radii in the interval $[1, 3]$. Then one can compute three points that pierce \mathcal{D} in $O(n)$ time.*

4.2.2 A 3/2-Approximation for the Maximum Clique in $G(\mathcal{D})$

We begin by computing the arrangement of the disks and, for each cell, identify a clique determined by the set of disks intersecting that cell. We next enumerate all non-Helly triples, which requires $O(n^3)$ guesses. For each such triple, we obtain three piercing points by Theorem 4.8. For every

pair of piercing points p, p' , we compute the maximum clique in the intersection graph induced by the disks pierced by p and p' . Finally, we return the largest clique among all the cliques that have been computed.

Theorem 4.9 *Given n disks with radii in $[1, 3]$, we can compute a clique C in their intersection graph G in $O(n^3 f(n))$ time such that $|C| \geq 2|M|/3$. Here M is a maximum clique in G and $f(n)$ is the time to find a maximum clique in an n -vertex bipartite graph.*

The theorem holds for any configuration of $[1, 3]$ -disks, and hence applies also in the scenario when all disks are stabbed by a line.

5 Conclusion

There are several avenues for future research. The case for stabbed segments with endpoints on $O(1)$ lines remains open. An intriguing direction is to establish APX-hardness or design a PTAS for upward ray graphs. One may also attempt to generalize the results we obtained for $[1, 3]$ -disks. It would be interesting to find better approximations with faster running time.

References

- [1] P. K. Agarwal and N. H. Mustafa. Independent set of intersection graphs of convex objects in 2D. *Computational Geometry*, 34(2):83–95, 2006.
- [2] R. Akpanya, B. Rivier, and F. B. Stock. Open problems from CCCG 2024. In *Proceedings of the 32nd Canadian Conference on Computational Geometry (CCCG)*, pages 167–170, 2024.
- [3] C. Ambühl and U. Wagner. The clique problem in intersection graphs of ellipses and triangles. *Theory of Computing Systems*, 38(3):279–292, 2005.
- [4] S. Bandyapadhyay, A. Maheshwari, S. Mehrabi, and S. Suri. Approximating dominating set on intersection graphs of rectangles and l-frames. *Computational Geometry*, 82:32–44, 2019.
- [5] J. Bang-Jensen, B. Reed, M. Schacht, R. Šámal, B. Toft, and U. Wagner. On six problems posed by jarik nešetřil. In *Topics in Discrete Mathematics: Dedicated to Jarik Nešetřil on the Occasion of his 60th Birthday*, pages 613–627. Springer, 2006.
- [6] A. Biniaz, P. Bose, and Y. Wang. Simple linear time algorithms for piercing pairwise intersecting disks. *Computational Geometry*, 114:102011, 2023.
- [7] M. Bonamy, É. Bonnet, N. Bousquet, P. Charbit, P. Giannopoulos, E. J. Kim, P. Rzazewski, F. Sikora, and S. Thomassé. EPTAS and subexponential algorithm for maximum clique on disk and unit ball graphs. *J. ACM*, 68(2):9:1–9:38, 2021.
- [8] M. Bonamy, E. Bonnet, N. Bousquet, P. Charbit, and S. Thomassé. EPTAS for max clique on disks and unit balls. In M. Thorup, editor, *Proceedings of the 59th IEEE Annual Symposium on Foundations of Computer Science (FOCS)*, pages 568–579. IEEE Computer Society, 2018.
- [9] É. Bonnet, P. Giannopoulos, E. J. Kim, P. Rzazewski, and F. Sikora. QPTAS and subexponential algorithm for maximum clique on disk graphs. In B. Speckmann and C. D. Tóth, editors, *Proceedings of the 34th International Symposium on Computational Geometry (SoCG)*, volume 99 of *LIPICS*, pages 12:1–12:15. Schloss Dagstuhl - Leibniz-Zentrum für Informatik, 2018.

[10] P. Bose, P. Carmi, J. M. Keil, A. Maheshwari, S. Mehrabi, D. Mondal, and M. Smid. Computing maximum independent set on outerstring graphs and their relatives. *Comput. Geom.*, 103:101852, 2022.

[11] H. Breu. *Algorithmic aspects of constrained unit disk graphs*. PhD thesis, University of British Columbia, 1996.

[12] S. Cabello. Maximum clique for disks of two sizes. *Open problems from Geometric Intersection Graphs: Problems and Directions CG Week Workshop, Eindhoven, June 25*, 2015.

[13] S. Cabello. Open problems presented at the algorithmic graph theory. *Adriatic Coast workshop, Koper, Slovenia, June 16–19*, 2015.

[14] S. Cabello, J. Cardinal, and S. Langerman. The clique problem in ray intersection graphs. In *European Symposium on Algorithms (ESA)*, pages 241–252. Springer, 2012.

[15] S. Cabello, J. Cardinal, and S. Langerman. The clique problem in ray intersection graphs. *Discret. Comput. Geom.*, 50(3):771–783, 2013.

[16] S. Cabello and M. Jejčič. Refining the hierarchies of classes of geometric intersection graphs. *The electronic journal of combinatorics*, pages P1–33, 2017.

[17] J. Cardinal, S. Felsner, T. Miltzow, C. Tompkins, and B. Vogtenhuber. Intersection graphs of rays and grounded segments. *J. Graph Algorithms Appl.*, 22(2):273–295, 2018.

[18] P. Carmi, M. J. Katz, and P. Morin. Stabbing pairwise intersecting disks by four points. *Discrete & Computational Geometry*, 70(4):1751–1784, 2023.

[19] D. Chakraborty, K. Gajjar, and I. Rusu. Recognizing geometric intersection graphs stabbed by a line. *Theoretical Computer Science*, 995:114488, 2024.

[20] T. M. Chan, T. C. van Dijk, K. Fleszar, J. Spoerhase, and A. Wolff. Stabbing rectangles by line segments—how decomposition reduces the shallow-cell complexity. In *Proceedings of the 29th International Symposium on Algorithms and Computation (ISAAC)*, 2018.

[21] B. N. Clark, C. J. Colbourn, and D. S. Johnson. Unit disk graphs. *Discret. Math.*, 86(1–3):165–177, 1990.

[22] L. Danzer. Zur lösung des gallaischen problems über kreisscheiben in der euklidischen ebene. *Studia Sci. Math. Hungar.*, 21(1-2):111–134, 1986.

[23] D. Eppstein and J. Erickson. Iterated nearest neighbors and finding minimal polytopes. *Discret. Comput. Geom.*, 11:321–350, 1994.

[24] P. Erdős and G. Szekeres. A combinatorial problem in geometry. *Compositio mathematica*, 2:463–470, 1935.

[25] J. Espenant, J. M. Keil, and D. Mondal. Finding a maximum clique in a disk graph. In E. W. Chambers and J. Gudmundsson, editors, *Proceedings of the 39th International Symposium on Computational Geometry (SoCG)*, volume 258 of *LIPICS*, pages 30:1–30:17. Schloss Dagstuhl - Leibniz-Zentrum für Informatik, 2023.

[26] S. Felsner, R. Müller, and L. Wernisch. Trapezoid graphs and generalizations, geometry and algorithms. *Discret. Appl. Math.*, 74(1):13–32, 1997.

[27] A. V. Fishkin. Disk graphs: A short survey. In K. Jansen and R. Solis-Oba, editors, *Proceedings of Approximation and Online Algorithms, First International Workshop (WAOA)*, volume 2909 of *Lecture Notes in Computer Science*, pages 260–264. Springer, 2003.

[28] J. Fox and J. Pach. Computing the independence number of intersection graphs. In D. Randall, editor, *Proceedings of the Twenty-Second Annual ACM-SIAM Symposium on Discrete Algorithms (SODA)*, pages 1161–1165. SIAM, 2011.

[29] F. Gavril. Maximum weight independent sets and cliques in intersection graphs of filaments. *Information Processing Letters*, 73(5-6):181–188, 2000.

[30] H. Hadwiger and H. Debrunner. *Ausgewählte Einzelprobleme der kombinatorischen Geometrie in der Ebene*. Kundig, 1955.

[31] V. Jelínek and M. Töpfer. On grounded L-graphs and their relatives. *Electr. J. Comb.*, 26(3):P3.17, 2019.

[32] J. M. Keil, J. S. Mitchell, D. Pradhan, and M. Vatshelle. An algorithm for the maximum weight independent set problem on outerstring graphs. *Computational Geometry*, 60:19–25, 2017.

[33] J. M. Keil and D. Mondal. The maximum clique problem in a disk graph made easy. In O. Aichholzer and H. Wang, editors, *Proceedings of the 41st International Symposium on Computational Geometry (SoCG)*, volume 332 of *LIPICS*, pages 63:1–63:16. Schloss Dagstuhl - Leibniz-Zentrum für Informatik, 2025.

[34] J. M. Keil, D. Mondal, E. Moradi, and Y. Nekrich. Finding a maximum clique in a grounded 1-bend string graph. *Journal of Graph Algorithms and Applications*, 26(4), 2022.

[35] J. Kratochvíl and J. Nešetřil. Independent set and clique problems in intersection-defined classes of graphs. *Commentationes Mathematicae Universitatis Carolinae*, 31(1):85–93, 1990.

[36] D. Kratsch and L. Stewart. Domination on cocomparability graphs. *SIAM Journal on Discrete Mathematics*, 6(3):400–417, 1993.

[37] G. Liu and H. Wang. Geometric hitting set for line-constrained disks. In *Algorithms and Data Structures Symposium*, pages 574–587. Springer, 2023.

[38] M. Löffler and M. van Kreveld. Largest bounding box, smallest diameter, and related problems on imprecise points. *Computational Geometry*, 43(4):419–433, 2010.

[39] M. Middendorf and F. Pfeiffer. The max clique problem in classes of string-graphs. *Discret. Math.*, 108(1-3):365–372, 1992.

[40] D. Mondal. Simultaneous embedding of colored graphs. *Graphs and Combinatorics*, 37(3):747–760, 2021.

[41] L. Stachó. A solution of gallai’s problem on pinning down circles. *Mat. Lapok*, 32(1-3):19–47, 1981.

A Construction of a Sail Skeleton

Assume that $k' = \lceil k/2 \rceil + 1$. We will ensure the sail-skeleton satisfies the following properties.

- P1. For each i from 1 to k' , the absolute values of the slopes of L_{2i-1} and L_{2i} are the same.
- P2. For each i from 2 to k' , the slope of L_{2i} is larger than $L_{2(i-1)}$.
- P3. For each i from 2 to $2k'$, the origin of L_i lies on L_{i-1} , and L_i intersects all other skeleton rays, i.e., $\{L_1, L_2, \dots, L_{2k'}\} \setminus L_i$.

We now describe an incremental construction for \mathcal{S}_ℓ and \mathcal{S}_r that satisfies the properties P1–P3. Assume that $\alpha = 90^\circ/2k'$ and let β be a small positive constant.

Let L_1 be the upward skeleton ray with origin at $(0, 0)$ and $(90^\circ + \alpha)$ angle of inclination with the positive x-axis. Let z be a point on L_1 . We define L_2 to be the skeleton ray with origin z and angle of inclination $(90^\circ - \alpha)$. It is straightforward to verify properties P1–P3 for $\{L_1, L_2\}$. For each i from 2 to k' , we set the angle of inclination of L_{2i-1} and L_{2i} to $(90^\circ + i\alpha)$ and $(90^\circ - i\alpha)$, respectively, which satisfies P1–P2. We now describe the origins of L_{2i-1} and L_{2i} and show that $\{L_1, L_2, \dots, L_{2i}\}$ satisfy P3.

Let $e_1^\ell, e_3^\ell, \dots, e_{2i-1}^\ell$ be the extremal path of \mathcal{S}_ℓ , and let $e_2^r, e_4^r, \dots, e_{2i-2}^r$ be the extremal path of \mathcal{S}_r . If i is even, then let p be a point on e_{2i-2}^r located at distance β from the lower endpoint of e_{2i-2}^r (e.g., the zoomed-in view of Figure 2(d)). We set the origin of L_{2i-1} as p . Since L_{2i-1} has a negative slope and L_2, \dots, L_{2i-2} have positive slopes, L_{2i-1} intersects all these skeleton rays with even indices. Since L_{2i-1} has a higher angle of inclination, it intersects all skeleton rays L_1, \dots, L_{2i-3} . Similarly, when i is odd, we set the origin of L_{2i} at a point on e_{2i-1}^r located at distance β from the lower endpoint of e_{2i-1}^r and show that it intersects all skeleton rays in $\{L_1, \dots, L_{2i-1}\}$. Consequently, property P3 becomes satisfied.

B Construction of a Non-degenerate Sail

Let $v_1, v_2, \dots, v_{|\sigma_j|}$ be the vertices of σ_j and let $r_1, r_2, \dots, r_{|\sigma_j|}$ be the corresponding rays. Initially all the rays pass through the centroid of $\xi(j+1)$ (Figure 12). We do not move the ray for v_1 and $v_{|\sigma_j|}$. For i from 2 to $|\sigma_j| - 1$, we move r_i closer to r_1 to form the edge e'_i by intersecting e'_{i-1} . Since we do not require polynomially bounded coordinates, this process yields the required non-degenerate sail.

C Construction of the Rays for the Internal Nodes of P

By the definition of admissible extension, each path in P has either one or two internal vertices. Furthermore, its end vertices are two leaves of T that are consecutive at the same level of T . Let a, b, c, d be a path in P , where b and c may coincide. Assume that a, d belong to the j th level of T . Let r_a, r_d be the rays of a and d , respectively. We insert the rays r_b and r_c (for b and c) when constructing R_{j+1} . Let e_a and e_d be the segments corresponding to r_a, r_d on the extremal path of R_j . Since a, d are consecutive in σ_j , the edges e_a, e_d are consecutive on the extremal path of R_j .

We set the origins of both r_b, r_c to a common point inside the cell immediately above e_a and e_d . Similar to the construction in the previous section, the rays initially pass through the centroid of $\xi(j+2)$. If $b \neq c$, then after constructing R_{j+1} , we shift r_c slightly by keeping it parallel to r_b . We ensure that the origin of r_c remains within the same cell and it intersects the identical set of rays

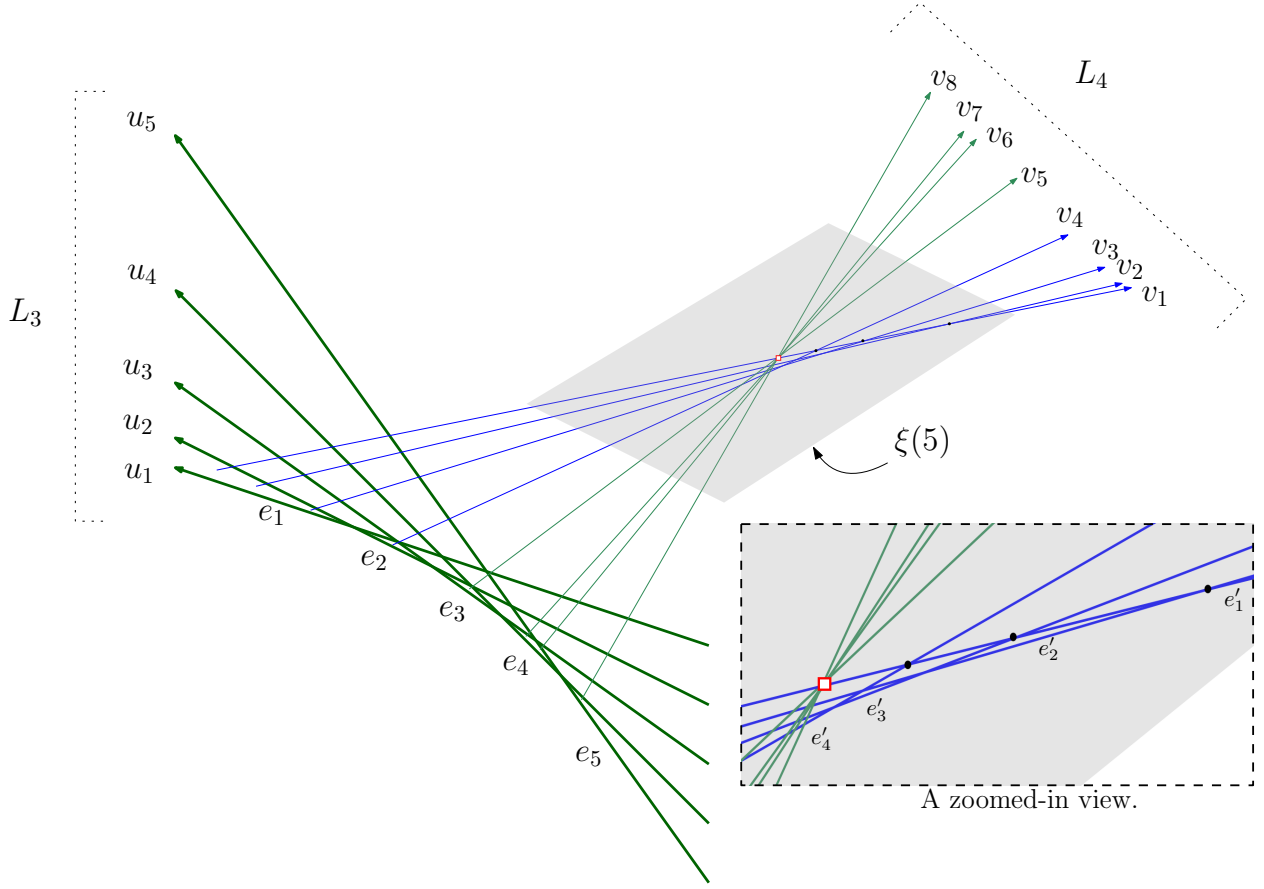


Figure 12: Illustration for the construction of a non-degenerate sail. Initially all the rays pass through the centroid of $\xi(5)$, which is marked in red square. The ray v_1 and v_8 stay at the same place. The rays v_2, v_3, \dots move closer to intersect v_1 above the centroid forming the extremal path. The three rays v_2, v_3, v_4 moved so far are shown in blue. The intersection points between v_1 and v_2, v_3, v_4 are shown in black dots.

as r_b (in the same order). For example, consider the path $(v_7, w_6, w_7, v_8) \in P$ in Figure 4, where the two rays of w_6, w_7 are parallel and originate inside the cell immediately above e_{v_7}, e_{v_8} .

It now suffices to show that the adjacencies of r_b and r_c in $\overline{(T \cup P)}$ have been realized correctly, i.e., they intersect all rays corresponding to $\sigma_1, \dots, \sigma_j$ except for the rays r_a, r_d . By the construction of the initial sail skeleton, r_b, r_c intersect all rays in $\sigma_1, \dots, \sigma_{j-2}$. Since r_b, r_c start at the cell immediately above e_a and e_d (e.g., the cell shaded in gray in the zoomed-in view of Figure 4), they intersect all rays corresponding to $\sigma_{j-1} \setminus \{r_b, r_c\}$. Since r_b, r_c initially pass through a common point of $\xi(j+2)$, they intersect all other rays in σ_{j+1} . The intersection graph remains the same during the perturbation that yields R_{j+1} . Finally, in the case when $b \neq c$, we made r_b and r_c parallel. Consequently, all adjacencies of b and c in $\overline{(T \cup P)}$ are correctly realized.

D Details of Section 3.1.1

Proof: [Proof of Lemma 3.1] Let r_1 and r_2 be two rays in $U(S)$ and let s_1 and s_2 be the corresponding segments in S' . If two segments in S intersect, then their rays r_1 and r_2 in $U(S)$ intersect. By construction, s_1 and s_2 satisfy $(C_1) - (C_2)$, i.e., they are strictly independent. Consider now the case

when s_1 and s_2 are strictly independent. By conditions (C_1) – (C_2) , extending the segments s_1 and s_2 beyond their free endpoints must create an intersection between the extended parts. Hence r_1 and r_2 must intersect and consequently, their associated segments in S intersect. \square

E Details of Section 3.1.2

Proof: [Proof of Lemma 3.2] We first show that $Z \cup (A \setminus A')$ is a strict independent set, i.e., every segment $s_p \in Z$ is strictly independent with every segment $s_q \in (A \setminus A')$. Since $(T \cup Z)$ is a strict independent set, we may assume that $s_q \notin T$. Without loss of generality let s_q be a segment of \overline{A}'_ℓ with the free endpoint on some line $\ell \in \{\ell_1, \dots, \ell_k\}$ (Figure 7(a)). Since $s_q \notin T$, T must contain two segments s_a and s_b , which are the highest and lowest segments of \overline{A}'_ℓ with free endpoints on ℓ . Suppose for a contradiction that s_p and s_q are not strictly independent.

Assume first that condition C_1 is violated, i.e., s_p intersects s_q . Since the segments s_a, s_q, s_b, s_i belong to A , they form a strict independent set. The segment s_i lies between s_q and s_p . Hence to avoid intersection with s_q and s_p , s_i must be smaller than s_p , which contradicts our assumption that $s_p \in Z$ because no segment of Z is higher than s_i, s_j .

Assume now that condition C_2 is violated. If the extended part of s_q intersects s_p , then s_p must be higher than s_i , which contradicts our assumption that $s_p \in Z$.

If the extension of s_p intersects s_q , then we show that s_p cannot be strictly independent with $\{s_a, s_b\}$, which contradicts that $(T \cup Z)$ is a strict independent set. Since s_a and s_b are strictly independent, they cannot lie on opposite halfplanes of ℓ , as this would violate condition C_2 . Consider now without loss of generality that s_a and s_b lie to the left halfplane of ℓ . We now consider the following two cases.

- Assume that s_a is to the left of s_q . Since s_a is not intersected by the extension of s_p , the free endpoint of s_a lies on the left halfplane of the line L_p determined by s_p , whereas the free endpoints of s_q and s_b lie on the right halfplane of L_p . Consequently, s_b must intersect s_p or its extension.
- If s_a is between s_q and s_p , then to avoid intersection with the extension of s_p , s_a must be smaller than s_q . This contradicts our assumption that s_q is smaller than s_a .

We have now proved that $Z \cup (A \setminus A')$ is a strict independent set. Since $Q[s_i, s_j, T]$ maximizes the number of segments that can be added to T such that the resulting set is strictly independent, $|Z|$ cannot be smaller than $|A'|$. If $|Z| > |A'|$, then it contradicts the assumption that A is a maximum strict independent set. Hence $Q[s_i, s_j, T]$ is equal to $|A'|$. \square

Proof: [Proof of Lemma 3.3] By definition, $Q[s_i, s_j, T]$ denotes the maximum number of segments from $\sigma[i+1 \dots j-1]$ that are no higher than s_i, s_j and can be added to T such that the resulting set is strictly independent. Therefore, in the base case, where no such segment exists, we set $Q[s_i, s_j, T]$ to 0.

We now consider the general step (Figures 7(b)–(d)). Let Z be the set of segments corresponding to $Q[s_i, s_j, T]$, which by definition forms strictly independent set with T . Let s_k be the highest segment of Z that is no higher than s_i, s_j . Let Z_ℓ and Z_r be the segments of Z that lie to the left and right of s_k , respectively. It now suffices to show that $Q[s_i, s_k, T_1] = |Z_\ell|$ and the segments corresponding to $Q[s_i, s_k, T_1]$ are strictly independent with Z_r . An analogous argument can be used to show $Q[s_i, s_k, T_2] = |Z_r|$. Together with s_k , we get the desired recurrence relation.

Since $s_k \in Z$, $(Z_\ell \cup \{s_k\})$ is a strict independent set. Since $(T_1 \setminus \{s_k\}) \subset T$, the set $(Z_\ell \cup (T_1 \setminus \{s_k\}))$ is strictly independent. Therefore, $(Z_\ell \cup T_1)$ is a strict independent set. Since s_k is a highest segment

in Z , no segment in Z_ℓ is higher than s_k . Observe that the segments corresponding to $Q[s_i, s_k, T_1]$ and Z_r lie to the left and right of s_k , respectively, and all these segments are strictly independent to s_k . Furthermore, none of these segments is higher than s_k . Therefore, the segments corresponding to $Q[s_i, s_k, T_1]$ are strictly independent with the set Z_r . By definition, $Q[s_i, s_k, T_1]$ maximizes the number of segments that satisfy the same height and strict independence properties as that of Z_ℓ . Therefore, $Q[s_i, s_k, T_1] \geq |Z_\ell|$. If $Q[s_i, s_k, T_1] > |Z_\ell|$, then we could delete Z_ℓ from Z and add all the segments corresponding to $Q[s_i, s_k, T_1]$ to Z to improve $Q[s_i, s_j, T]$, which contradicts our initial assumption about the optimality of $Q[s_i, s_j, T]$. \square

F Details of Section 3.3

Proof: [Proof of Theorem 3.8] Let S be a set of n grounded segments and let $G(S)$ be the corresponding intersection graph. Assume that the free endpoints of the segments are in general position, i.e., no two share the same x - or y -coordinates and no segment contains an endpoint of another segment. Let F be the sequence of free endpoints in increasing order of x -coordinates. By Erdős-Szekeres theorem [24], there exists a subsequence of $\Omega(\sqrt{n})$ free endpoints in F that have either monotonically increasing or decreasing y -coordinates. One can use this result to obtain a partition of F into subsequences F_1, \dots, F_k , where $k = O(\sqrt{n})$, and every F_i , where $1 \leq i \leq k$, contains at most \sqrt{n} elements [40]. Similarly, we partition the segments of each F_i into a set of subsequences $\sigma_{i,1}, \dots, \sigma_{i,z}$, where $z = O(\sqrt[4]{n})$, and for each $\sigma_{i,j}$, where $1 \leq j \leq k$, the x -coordinates of its segments on the ground line are either increasing or decreasing.

Let M be a maximum clique in $G(S)$. Then there exist indices i, j , such that $\sigma_{i,j}$ contains at least $\frac{|M|}{zk} = \Omega(n^{-3/4}|M|)$ vertices of M . Let $M(\sigma_{i,j})$ be the maximum clique in the intersection graph corresponding to the segments of $\sigma_{i,j}$. Then $|M(\sigma_{i,j})| \geq \frac{|M|}{zk}$. We now show that $M(\sigma_{i,j})$ is cocomparability graph and hence it suffices to return a clique found over all subsequences.

By Lemma 3.5, it suffices to show that $\sigma_{i,j}$ is an umbrella-free ordering for the intersection graph corresponding to $\sigma_{i,j}$, and hence $M(\sigma_{i,j})$ can be computed in polynomial time [29]. Let s_p, s_q, s_r be three segments in this order in $\sigma_{i,j}$. Assume for a contradiction that s_p and s_r intersect, but none of them intersects s_q . Since $\sigma_{i,j}$ is a subsequence of F_i , the free endpoints s_p^t, s_q^t, s_r^t are monotonically increasing or decreasing. Therefore, the y -coordinate of s_q^t is in between the y -coordinates of s_p^t and s_r^t . Let Δ be the triangle determined by the segments s_p, s_r and the ground line. Note that s_q lies between s_p and s_r on the ground line. Since s_q neither intersects s_p nor s_r , it lies interior to Δ , which contradicts that the y -coordinate of s_q^t is in between the y -coordinates of s_p^t and s_r^t . \square

G Details of Section 3.2

Remark G.1 Let Δabc be a triangle with base ab and peak c . Let q be a point on the segment ab . Then $|qc| \leq \max\{|ac|, |bc|\}$.

Proof: [Proof of Lemma 3.6] Let $\sigma = (s_\ell, \dots, s_r)$ be the order of the segments on the ground line. Note that by definition, all the segments in $G(s_\ell, s_r)$ intersect both s_ℓ and s_r . We now show that σ is an umbrella-free ordering for $G(s_\ell, s_r)$, and thus $G(s_\ell, s_r)$ is a cocomparability graph by Lemma 3.5. Specifically, let s_a, s_c, s_b be three segments that appear in σ in this order. We now show that if s_a and s_b intersect, then at least one of them must intersect s_c .

For a segment s_a , we refer to its endpoint on the ground line as s_a^g and the free endpoint as s_a^t . If a pair of segments s_a and s_b intersect, then we denote the intersection point as $i(s_a, s_b)$. Let W

be the closed wedge-shaped region above the the two lines determined by s_ℓ and s_r . We distinguish two cases depending on whether $i(s_a, s_b)$ lies in W .

Case 1 ($i(s_a, s_b) \in W$). Suppose for a contradiction that s_c does not intersect s_a and s_b . Since s_c lies between s_a and s_b , the point s_c^t must be inside the triangle $\Delta s_a^g i(s_a, s_b) s_b^g$. Since s_c intersects both s_ℓ and s_r , s_c^t belongs to W . Without loss of generality assume that extending the segment s_c upward intersects s_b at a point w (Figure 8(a)). We now move w along s_b so that the length $|ws_c^g|$ increases. If w moves upward along s_b , then it reaches $i(s_a, s_b)$. We now apply Remark G.1 on $\Delta s_a^g i(s_a, s_b) s_b^g$ to observe that $|ws_c^g|$ is at most one unit. Since the length of s_c is strictly smaller than $|ws_c^g|$, s_c cannot be of unit length. If w moves downward along s_b , then it reaches $i(s_\ell, s_b)$. Note that we may also hit $i(s_r, s_b)$ while moving w , but we keep moving until we reach $i(s_\ell, s_b)$ (Figure 8(b)). We now can use the same argument by applying Remark G.1 on $\Delta s_\ell^g i(s_\ell, s_b) s_b^g$.

Case 2 ($i(s_a, s_b) \notin W$). If $i(s_a, s_b) \in \Delta s_\ell^g i(s_\ell, s_r) s_r^g$, then this triangle contains $\Delta s_a^g i(s_a, s_b) s_b^g$ (Figure 8(c)). Since s_c lies between s_a and s_b , s_c cannot reach the segments s_ℓ and s_r . If $i(s_a, s_b) \notin \Delta s_\ell^g i(s_\ell, s_r) s_r^g$, then without loss of generality assume that $i(s_a, s_b)$ lies below the line determined by s_ℓ (Figure 8(d)). Since $\Delta s_a^g i(s_a, s_b) s_b^g$ lies below the line determined by s_ℓ , s_c cannot intersect s_ℓ . \square

H Details of Section 4.1

Proof: [Proof of Theorem 4.1] For each disk $D \in \mathcal{D}$, we compute a maximum clique $M(D)$ that contains D as its smallest disk. A maximum clique of $G(\mathcal{D})$ is then obtained by taking the largest among these cliques. To compute $M(D)$, we can only examine the set of disks $S \subseteq \mathcal{D}$ that intersect D (Figure 13(a)). It now suffices to show that the intersection graph of S is a cobipartite graph. Let $S_\ell \subset S$ be the disks such that for each disk $D' \in S$, the x -coordinate of D' is at most that of the center of D . Let S_r to be the set of remaining disks of S . We now show that the disks in S_ℓ mutually intersect, and By symmetry, the same argument applies to S_r .

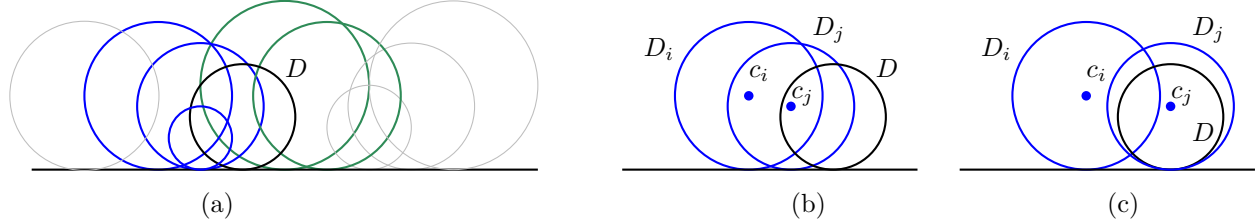


Figure 13: Illustration for Theorem 4.1. (a) \mathcal{D} , where D, S_ℓ and S_r are shown in black, blue and green, respectively. (b)–(c) Illustration for moving D_j to contain D .

Let $D_i, D_j \in S_\ell$ be two disks with radii r_i and r_j , and centers c_i and c_j , respectively. Let d be the Euclidean distance between c_i and c_j . Assume without loss of generality that the x -coordinate of c_i is at most the x -coordinate of c_j . We move D_j horizontally such that the x -coordinate of c_j becomes equal to that of D . Let d' be the new distance between D_i and D_j . We now observe that $d' \geq d$. Since D is the smallest disk and both D_j and D are grounded, D_j now entirely covers D (Figures 13(b)–(c)). Since D_i intersects D , it must intersect D_j , i.e., $d' \leq r_i + r_j$. Since $d \leq d'$, D_i must intersect D_j in their original positions. \square

I Details of Section 4.2.1

Proof: [Proof of Lemma 4.3] The proof follows since every point t on pc_2 is closer to c_1 than c_2 . \square

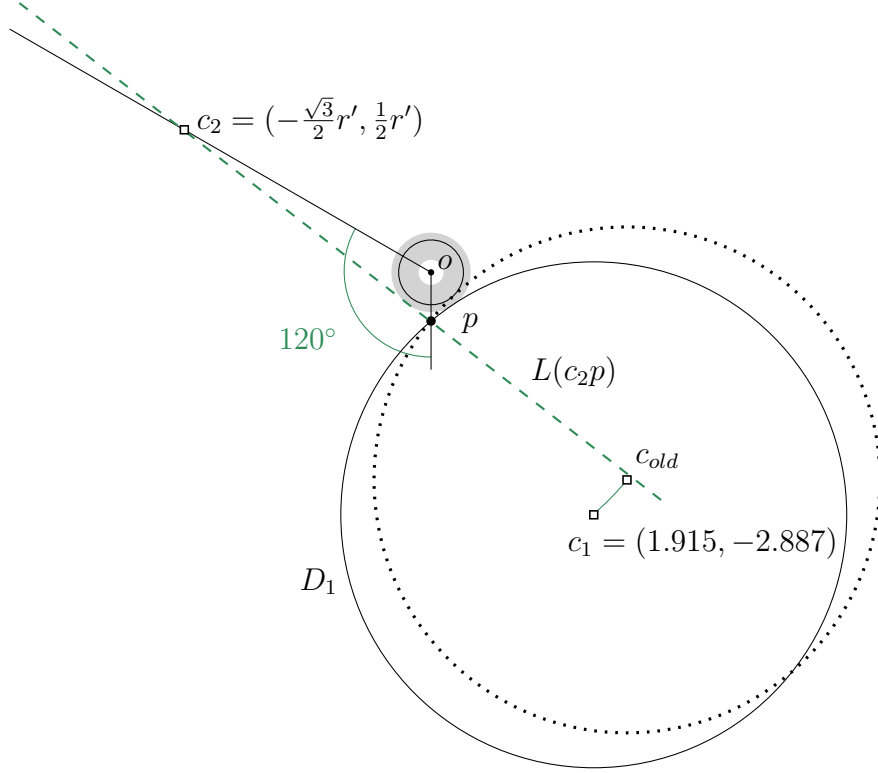


Figure 14: Illustration for Lemma 4.5. The gray annulus illustrates the range for M . The dotted disk is the position of D_1 before rotation.

Proof: [Proof of Lemma 4.4] Let R be the region of D_1 that lies outside D_2 . Since two distinct circles can intersect in at most two points, R is connected. Let C' be the largest arc on the boundary of D_1 that also lies on R . Since $r \notin D_2$, we have $r \in R$ and hence the arc C coincides with C' . \square

Proof: [Proof of Lemma 4.5] Suppose for a contradiction that D_1 and D_2 intersect. Let c_i be the center of D_i , where $i \in \{1, 2\}$. Let D be a disk containing D_1 that touches p and M and has radius three. Since D_1 and D_2 intersect and both avoid o , D must intersect D_2 . Therefore, we assume without loss of generality that D_1 is of radius three, and similarly D_2 is of radius three.

Note that D_1 and D_2 both avoid containing o , and D_1 touches p and M . If c_1 lies above $L(c_2p)$, then the part of D_1 below $L(c_2p)$ lies below the line that passes through p and perpendicular to $L(c_2p)$. Since we assume D_1 intersects D_2 below the line $y = -\frac{x}{\sqrt{3}}$, c_1 must lie on or below $L(c_2p)$.

Figure 14 illustrates the configuration. Increasing the radius of M keeps c_2 on line $y = -x/\sqrt{3}$, but moves c_1 further away from o , which keeps c_1 below $L(c_2p)$. We now rotate D_1 clockwise such that it touches p and $|c_1o|$ becomes $3(\frac{2}{\sqrt{3}} - 1)$. Let c_{old} be the position of c_1 before the rotation. Let Z be a circle with center c_2 and radius c_{old} . Since p lies inside Z , and on or above $L(c_{old}c_2)$, c_1 lies inside Z . Therefore, D_1 still intersects D_2 after rotation.

We now have c_1 at $(1.915, -2.887)$, which can be obtained from the equations $x^2 + (y + \frac{1}{\sqrt{3}})^2 = 9$ and $x^2 + y^2 = r'^2$, where $r' = 3 + r(\frac{2}{\sqrt{3}} - 1)$. The center c_2 is at $(-\frac{\sqrt{3}}{2}r', \frac{1}{2}r')$. We now have $|c_1c_2| = \sqrt{(1.915 + \frac{\sqrt{3}}{2}r')^2 + (-2.887 - \frac{1}{2}r')^2}$. For $r \in [1, 3]$, we have $|c_1c_2| \in [6.44, 6.74]$, which contradicts the assumption that D_1 and D_2 intersect. \square

I.1 Details of Case 2

Case 2.1 (D' intersects D_ℓ below $L(oC)$). Let r_ℓ be the radius of D_ℓ . We first translate D' such that it touches A and Q and also maintains the intersection with D_ℓ , as follows. We translate D' along oc' until it touches A , which keeps the intersection with Q . By Lemma 4.3, D' continues to intersect D_ℓ . Since c_ℓ in the second quadrant (Lemma 4.7) and D_ℓ avoids o , D_ℓ cannot contain A . Since D_ℓ and D' both avoid A , and since D_ℓ and D' intersect below $L(oC)$, A is above $L(c'c_\ell)$. We now rotate D' clockwise such that the distance $|c'A|$ remains fixed but c' touches Q (Figure 15(a)). Let c'_{old} be the position of c' before rotation. Consider a point A' where $|c'_{old}A'| = |c'A'| = |c_\ell c'|$ (Figure 15(b)). Since A lies above $L(c_\ell c'_{old})$, A' lies above $L(c_\ell c'_{old})$. Moving A' to c_ℓ without changing the distance $|A'c'_{old}|$ decreases the angle $\angle c'c'_{old}A'$. We now consider the angles of $\Delta c'A'c_{old}$ to observe that $|c_\ell c'| \leq |c_\ell c_{old}|$. Therefore, after rotation, D' continues to intersect D_ℓ .

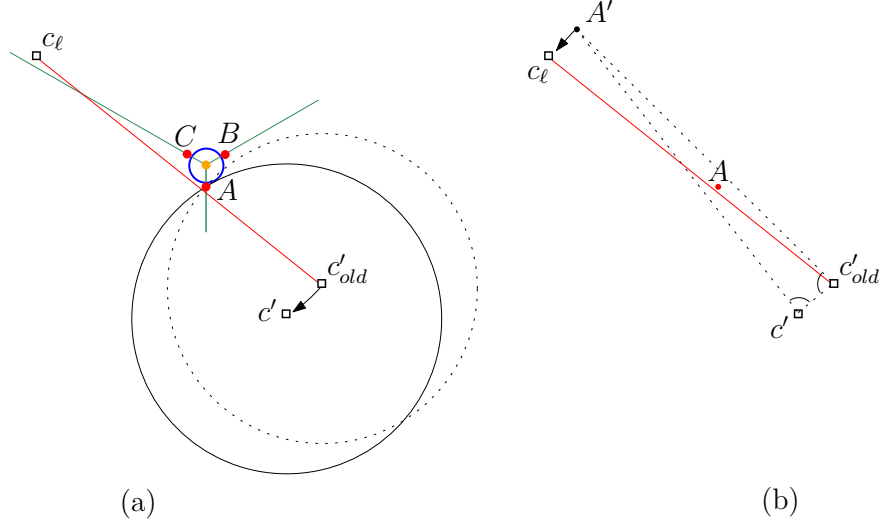


Figure 15: Illustration for moving D' to touch A and Q . The origin o is in orange.

We now define a disk D'' with center c'' and radius three that touches A and has its center on $L(oc')$. Since D'' contains the part of D' to the left of $L(oA)$, D'' intersects D_ℓ (Figure 16(a)). Since the largest radius among the disks of \mathcal{D} is three, the radius of Q is at most $3(\frac{2}{\sqrt{3}} - 1)$ (Lemma 4.2). We now rotate D'' clockwise around A such that the distance $|oc''|$ becomes $3 + 3(\frac{2}{\sqrt{3}} - 1)$. We can now use the same argument that we used for rotating D' to observe that D'' continues to intersect D_ℓ . Since $(\frac{2}{\sqrt{3}} - 1) \leq r_q \leq 3(\frac{2}{\sqrt{3}} - 1) \approx 0.46$ and since D'' touches A , one can observe that c'' lies in the fourth quadrant.

We now consider two scenarios based on the position of c_ℓ . Assume first that the center of c_ℓ lies above $L(oC)$. We roll D_ℓ over Q counter-clockwise such that its center c_ℓ lies on $L(oC)$. Since c_ℓ lies at the second quadrant (Lemma 4.7), rolling over Q decreases the y -coordinate of c_ℓ (Figure 16(b)). Let c_{old} be the position of c_ℓ before moving D_ℓ . Then $\angle c_\ell c_{old}c'' \leq \angle c'' c_\ell c_{old}$, and hence D_ℓ continues to intersect D' . We now apply Lemma 4.5 considering D'' and D_ℓ as D_1 and D_2 to reach a contradiction.

Assume now that c_ℓ lies below $L(oC)$. Lemma 4.7 implies that D_ℓ touches the *upper-left arc* of D_b , i.e., the clockwise arc on the boundary from the leftmost point to the topmost point of D_b . We now show that the upper-left arc of D_b is outside of D'' , which contradicts that D'' intersects D_ℓ (Figure 16(c)).

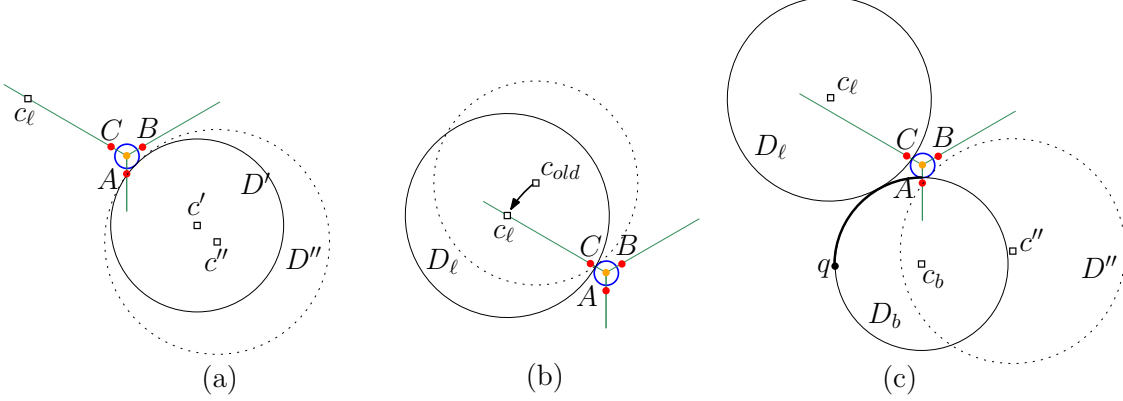


Figure 16: The origin o is in orange. Illustration showing (a) D'' (b) D_ℓ rolls over Q , and (c) q lies outside of D'' .

We first compute the center $c'' = (x, y)$ of D'' . Since c'' is at distance $3 + 3(\frac{2}{\sqrt{3}} - 1) = 2\sqrt{3}$ from o , we have $x^2 + y^2 = (2\sqrt{3})^2$. Furthermore, c'' is at distance 3 from A , and hence $x^2 + (y + \frac{1}{\sqrt{3}})^2 = 3^2$. Consequently, $c'' \approx (1.915, -2.887)$. Let r_b be the radius of D_b . The distance between c'' and the leftmost point $q = (-r_b, -r_b - \frac{1}{\sqrt{3}})$ of D_b is $|c''q| \approx \sqrt{(r_b + 1.915)^2 + (r_b - 2.310)^2}$, which is larger than 3.19 for every $r_b \geq 1$. Therefore, D'' cannot contain q . By Lemma 4.4, the upper-left arc of D_b lies outside of D'' , as required.

Case 2.2 (D' intersects D_ℓ above $L(oC)$). If c_ℓ lies below $L(oC)$, then we use the same argument of Case 2.1 when c_ℓ is above $L(oC)$. Specifically, we move D' to touch B and Q , and roll D_ℓ over Q such that c_ℓ lies on $L(oC)$ to apply the arguments of Case 2.1 (Figure 17(a)).

We now assume that c_ℓ lies above $L(oC)$ and $c' \in W(\angle BoA)$. Consider the triangle $\Delta c_b o c_\ell$ where $|c_\ell o| = r_\ell + r_q$, $|c_b o| = r_b + r_q$ and $|c_\ell c_b| = r_\ell + r_b$ (Figure 17(b)). The angle $\angle c_b o c_\ell = \arccos\left(\frac{(r_\ell + r_q)^2 + (r_b + r_q)^2 - (r_\ell + r_b)^2}{2(r_\ell + r_q)(r_b + r_q)}\right) = \arccos\left(\frac{r_\ell r_q + r_b r_q + r_q^2 - r_\ell r_b}{(r_\ell + r_q)(r_b + r_q)}\right) = \arccos\left(1 - \frac{2r_\ell r_b}{(r_\ell + r_q)(r_b + r_q)}\right)$. For a fixed r_ℓ, r_b , the angle increases when r_q decreases. For fixed r_q , the angle increases when r_ℓ and r_b increase. Therefore, $\angle c_b o c_\ell$ is maximized when $r_q = (\frac{2}{\sqrt{3}} - 1)$ and $r_\ell = r_b = 3$, and hence $\angle c_b o c_\ell \approx 143.97^\circ$.

Similar to Case 2.1, we show the existence of a disk D'' with center c'' and radius three that touches B , has distance $|oc''| = 3 + r_q$ and intersects D_ℓ . If $r_q = 3(\frac{2}{\sqrt{3}} - 1)$, then c'' is approximately $(3.457, -0.215)$ with $L(oc'')$ making an angle -3.56° with positive x-axis. Hence it suffices to consider the coordinate of $c'' = (|oc''| \cos \theta, -|oc''| \sin \theta)$, where $0^\circ \leq \theta \leq 90^\circ$.

We now roll D_ℓ over Q clockwise such that c_ℓ lies on the line L with angle of inclination 143.97° (Figure 17(c)). Since D_ℓ intersects D'' above $L(oC)$, c_ℓ must lie above $L(oc'')$. Hence D_ℓ continues to intersect D'' . Let D'_ℓ be a disk of radius three tangent to Q at the point where D_ℓ touches Q . Since D'_ℓ contains D_ℓ , it intersects D'' . Since the center c'_ℓ of D'_ℓ lies on $L(oc_\ell)$, $\angle c_b o c'_\ell \leq 143.97^\circ$. Therefore, we may assume that the center c'_ℓ has the coordinate $(-r \cos 53.97^\circ, r \sin 53.97^\circ)$, where $r = 3 + r_q$ (Figure 17(c)).

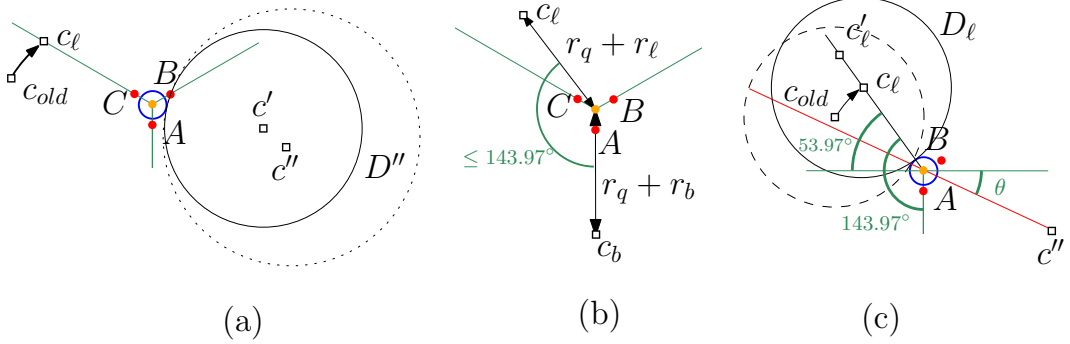


Figure 17: Illustration for Case 2.2. (a) The setup when c_ℓ lies below $L(oC)$. (b)–(c) The center c_ℓ lies above $L(oC)$.

We now reach a contradiction by showing $|c'_\ell c''|$ is larger than six, as follows.

$$\begin{aligned}
 |c'_\ell c''| &= \sqrt{(-r \cos 53.97^\circ - |oc''| \cos \theta)^2 + (r \sin 53.97^\circ + |oc''| \sin \theta)^2} \\
 &= \sqrt{r^2 + |oc''|^2 + 2r|oc''| \cos 53.97^\circ \cos \theta + 2r|oc''| \sin 53.97^\circ \sin \theta} \\
 &= \sqrt{r^2 + |oc''|^2 + 2r|oc''| \cos(53.97^\circ - \theta)} \\
 &= \sqrt{2r^2 + 2r^2 \cos(53.97^\circ - \theta)}
 \end{aligned}$$

If $r_q = 2(\frac{2}{\sqrt{3}} - 1)$, then $c'' \approx (3.039, -1.308)$ with $L(oc'')$ making an angle -23.3° with positive x-axis. Therefore, if $(\frac{2}{\sqrt{3}} - 1) \leq r_q < 2(\frac{2}{\sqrt{3}} - 1)$, then $23.3^\circ \leq \theta \leq 90^\circ$. The distance $|c'_\ell c''|$ is minimized when $\theta = 90^\circ$. Since distance decreases as r_q decreases, we have $|c'_\ell c''| \geq \sqrt{2(3 + (\frac{2}{\sqrt{3}} - 1))^2(1 + \cos 36.03^\circ)} > 6$.

If $2(\frac{2}{\sqrt{3}} - 1) \leq r_q \leq 3(\frac{2}{\sqrt{3}} - 1)$, then $0^\circ \leq \theta \leq 23.3^\circ$. The distance $|c'_\ell c''|$ is minimized when $\theta = 23.3^\circ$. Since distance decreases as r_q decreases, we have $|c'_\ell c''| \geq \sqrt{2(3 + 2(\frac{2}{\sqrt{3}} - 1))^2(1 + \cos 23.3^\circ)} > 6$.